The Egiin Davaa prehistoric rupture, central Mongolia: a large magnitude normal faulting earthquake on a reactivated fault with little cumulative slip located in a slowly deforming intraplate setting

R. T. WALKER[1]*, K. W. WEGMANN[2], A. BAYASGALAN[3], R. J. CARSON[4], J. ELLIOTT[1], M. FOX[5,6], E. NISSEN[7], R. A. SLOAN[1], J. M. WILLIAMS[4] & E. WRIGHT[8]

[1]*COMET, Department of Earth Sciences, University of Oxford, South Parks Road, Oxford OX1 3AN, UK*

[2]*Department of Marine, Earth and Atmospheric Sciences, North Carolina State University, Raleigh, NC 27695, USA*

[3]*School of Geology and Petroleum Engineering, Mongolian University of Science and Technology, Ulaanbaatar, Mongolia*

[4]*Department of Geology, Whitman College, Walla Walla, WA 99362, USA*

[5]*Department of Earth and Planetary Science, University of California, Berkeley, CA 94720, USA*

[6]*Berkeley Geochronology Center, 2455 Ridge Road, Berkeley, CA 94707, USA*

[7]*Department of Geophysics, Colorado School of Mines, 150 Illinois Street, Golden, CO 80401, USA*

[8]*Department of Geology, Colorado College, Colorado Springs, CO 80903, USA*

**Correspondence: richard.walker@earth.ox.ac.uk*

Abstract: The prehistoric Egiin Davaa earthquake rupture is well-preserved in late Quaternary deposits within the Hangay Mountains of central Mongolia. The rupture is expressed by a semi-continuous 80 km-long topographic scarp. Geomorphological reconstructions reveal a relatively constant scarp height of 4–4.5 m and a NW-directed slip vector. Previous researchers have suggested that the scarp's exceptional geomorphological preservation indicates that it may correspond to an earthquake that occurred in the region *c.* 500 years ago. However, we constrain the last rupture to have been at least 4 ka ago from morphological dating and <7.4 ka ago based on radiocarbon dating from one of two palaeoseismic trenches. Our study shows that discrete earthquake ruptures, along with details such as the locations of partially infilled fissures, can be preserved for periods well in excess of 1000 years in the interior of Asia, providing an archive of fault movements that can be directly read from the Earth's surface over a timescale appropriate for the study of slowly deforming continental interiors. The Egiin Davaa rupture involved *c.* 8 m of slip which, along with the observations that it is largely unsegmented along its length and that the ratio of cumulative slip (*c.* 250 m) to fault length (*c.* 80 km) is small, suggests relatively recent reactivation of a pre-existing geological structure.

Supplementary material: All scarp profiles are available at http://www.geolsoc.org.uk/SUP18871

This paper considers the potential for large magnitude earthquakes within continental interiors on faults that may have very low slip rates and little in the way of cumulative displacement. We focus on the Egiin Davaa prehistoric normal faulting earthquake from central Mongolia (e.g. Khil'ko *et al.* 1985; Baljinnyam *et al.* 1993), which formed a semi-continuous rupture 80 km in length and for which we estimate a magnitude of 7.3–7.7. Despite its size, the rupture occurred in the Cenozoic

From: LANDGRAF, A., KÜBLER, S., HINTERSBERGER, E. & STEIN, S. (eds) 2017. *Seismicity, Fault Rupture and Earthquake Hazards in Slowly Deforming Regions*. Geological Society, London, Special Publications, **432**, 187–212.
First published online November 18, 2015, updated December 13, 2016, https://doi.org/10.1144/SP432.4

along an ancient fault with <300 m of cumulative throw. A study of the Egiin Davaa rupture is hence important for understanding the potential for large destructive earthquakes on faults with little or no expression and for investigating the processes of fault initiation and reactivation.

Well-documented examples of large normal faulting earthquakes include the 1556 Huaxian earthquake of central China, which may have involved a throw of *c.* 8 m along a *c.* 100 km-long rupture (e.g. Yuan *et al.* 1991), and the 1739 Yinchuan earthquake, which generated a scarp with a maximum throw of *c.* 4.5 m over a length of *c.* 100 km (e.g. Zhang *et al.* 1986; Deng & Liao 1996). More recently, the 1959 Hebgen Lake (M_w 7.3) and 1983 Borah Peak (M_w 6.9) earthquakes of the western USA involved peak slips of 6 and 2.7 m, respectively (e.g. Stover & Coffman 1993). Most recently, the M_w 7.1 Yutian earthquake in Tibet generated surface offsets of 3–4 m over a rupture length of 45 km (Elliott *et al.* 2010). However, in contrast with the Egiin Davaa rupture, all of these examples occurred on faults with large cumulative displacements, the activity of which in the late Quaternary can be inferred with relative ease from the geomorphology.

The study of large earthquakes within slowly deforming continental interiors is challenging because modern examples are rare and the interval between successive earthquakes can be very long. Reconstructions of earthquakes from historical and prehistoric records are hence required to understand parameters such as the slip-vector azimuth and estimated magnitude. Moreover, by reconstructing ancient earthquakes and by determining their slip vectors, we may be able to glean insights into the kinematics of faulting (i.e. the way in which the population of active faults accommodates the overall tectonic motions) in these slowly deforming regions.

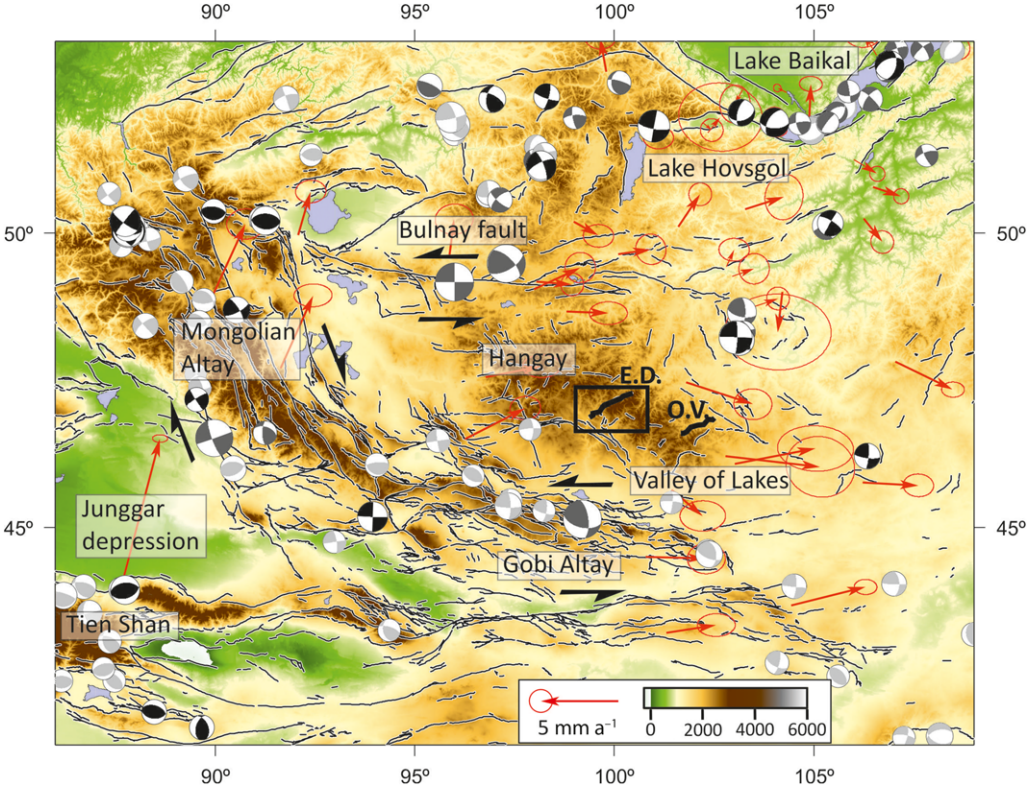

Fig. 1. Shaded relief Shuttle Radar Topography Mission (Farr & Kobrick 2000) topography of Mongolia showing active faults (updated from Walker *et al.* 2008). Earthquake focal mechanisms are from Bayasgalan *et al.* (2005). Waveform modelled focal mechanisms are shown in black, those determined from first arrivals in dark grey and Global CMT solutions in light grey. GPS velocities are shown relative to Siberia (Calais *et al.* 2003). The Egiin Davaa (E.D.) and Orhon Valley (O.V.) faults are highlighted as thick black lines. The black box outlines the region of this investigation as shown in Figure 2.

Using records of prehistoric earthquakes to investigate the kinematics of faulting is critical for investigations of the active tectonics of Mongolia (Fig. 1), where the faults are typically very long (100 km or greater), earthquake magnitudes can be large ($M_w > 7$) and the slip rates are typically slow, leading to very long recurrence intervals (e.g. Frankel *et al.* 2010; Rizza *et al.* 2011). In addition, the historical record of earthquakes in Mongolia is fragmentary and few were documented before the twentieth century. In compensation for the general lack of instrumentally recorded earthquakes across large parts of Mongolia, we are aided in the study of prehistoric earthquakes by the preservation of their surface ruptures in the landscape for long periods of time (e.g. Khil'ko *et al.* 1985; Baljinnyam *et al.* 1993; Walker *et al.* 2008). Few of the prehistoric ruptures have been dated directly, an exception being the Jid fault palaeorupture in western Mongolia, the age of which is bracketed at 970–850 years (Walker *et al.* 2006).

This study presents the results of 80 km of fault mapping, topographic profiling and the interpretations of two palaeoseismic sites along the Egiin Davaa normal fault within the Hangay Mountains of central Mongolia (Fig. 1). Evidence for Quaternary faulting is widespread within the Hangay Mountains, but there is no record of large earthquakes in the instrumental record (Fig. 1; Cunningham 2001; Walker *et al.* 2008). The Egiin Davaa fault is one of several normal faults within the Hangay Mountains (e.g. Baljinnyam *et al.* 1993; Cunningham 2001; Walker *et al.* 2007, 2008). It is expressed as a scarp in late Quaternary surfaces with a typical height of 4.5 m. The sharp geomorphology and continuity of displacement across and along the fault has led some researchers to the interpretion that it formed in a single earthquake rupture potentially related to an historical event recorded in the sixteenth century (e.g. Khil'ko *et al.* 1985; Baljinnyam *et al.* 1993).

In the following sections, we assess whether the Egiin Davaa fault scarp was likely to have been caused by a single earthquake and we provide estimates of its likely magnitude, age and slip direction. We also assess the variation of displacement along its length and evidence for segmentation. To achieve these aims, we combined evidence from the geomorphology (as observed in the field and from high-resolution KOMPSAT-2 satellite imagery), the offset on late Miocene basalt flows, palaeoseismic trenching and the analysis of topographic profiles measured orthogonal to the scarp.

Tectonic setting

The active tectonics of Mongolia are related to the ongoing India–Eurasia continental collision (Baljinnyam *et al.* 1993). Approximately 7 mm a^{-1} of NNE-directed shortening occurs across the Mongolian Altay Mountains in the western part of the country (Calais *et al.* 2003; Fig. 1). This shortening is accommodated on a series of NNW–SSE right-lateral strike-slip faults that are thought to rotate about a vertical axis (Bayasgalan *et al.* 2005). However, in central Mongolia, global positioning system (GPS) measurements indicate distributed east–west left-lateral shearing (Calais *et al.* 2003). The GPS measurements are compatible with the east–west left-lateral faulting observed across central Mongolia and there is hence no requirement for vertical axis rotation in this region (Bayasgalan *et al.* 2005).

The Hangay Dome sits in central Mongolia between two prominent zones of east–west striking left-lateral faults: the Gobi–Altai to the south and the Bulnay fault to the north (Fig. 1). The Bulnay fault zone was responsible for two earthquakes of M_w 8+ in 1905 (e.g. Baljinnyam *et al.* 1993; Schlupp & Cisternas 2007; Rizza *et al.* 2015) and *c.* 250 km of the Bogd fault in the Gobi–Altay ruptured in 1957 (e.g. Florensov & Solonenko 1965; Baljinnyam *et al.* 1993; Kurushin *et al.* 1997; Rizza *et al.* 2011). In contrast with its surroundings, the interior of the Hangay Dome has experienced no significant instrumentally recorded earthquakes (Fig. 1) and hence the distribution and style of active faulting is relatively poorly resolved compared with its surroundings.

The Hangay Mountains cover an area of over 200 000 km^2, with peaks up to 4000 m elevation and with valley incision of up to 1 km. The NW–SE-trending drainage divide separates rivers that flow northwards to Lake Baikal (and eventually to the Arctic Ocean) from those that flow southwards to the Valley of Lakes. The range is dome-shaped and many of the summits preserve remnants of a presumed pre-Cenozoic erosion surface (a peneplain) cut into resistant Palaeozoic sediments and late Palaeozoic–early Mesozoic granitoids (Cunningham 2001). West *et al.* (2013) fitted a surface across the peneplain remnants, hence removing the short-wavelength topography associated with valley incision into the surface. No large discontinuity is observed within the surface, indicating that any fault movements within the Hangay area have only a secondary effect on shaping its topography.

Neither the timing nor the cause of doming in the Hangay Mountains is well constrained. An increase in clastic sedimentation in the surrounding basins at 25–30 Ma is inferred to mark the onset of doming (Yanshin 1975; Cunningham 2001). The surface uplift may be associated with dynamic support from a mantle plume (Windley & Allen 1993), although the absence of a regional gravity anomaly across the Hangay region argues against such

support (Bayasgalan *et al.* 2005). It could also be associated with buoyancy from melting associated with lateral flow around the Precambrian crustal keel (Cunningham 2001) or by magmatic underplating of the crust (Petit *et al.* 1998). Tertiary and Quaternary volcanism is widespread within the Hangay region (e.g. Filippov *et al.* 1976; Barry *et al.* 2003; Ionov 2007; Yarmolyuk *et al.* 2008; Hunt *et al.* 2012; Ancuta *et al.* 2013).

Both strike-slip and normal faults occur within the Hangay region. Many of the active faults have slip vectors consistent with the regional east–west left-lateral shearing measured by GPS (Calais *et al.* 2003). Walker *et al.* (2007, 2008) identified a number of east–west left-lateral fault systems, all showing evidence of activity in the late Quaternary, within the western and southern parts of the Hangay Mountains (Fig. 1). The occurrence of active normal faults at high elevations is likely to be influenced by the high topography within the range (Cunningham 2001). However, there is uncertainty as to whether the slip vectors on the normal faults are consistent with the regional strain field or whether they respond purely to the local extensional stresses associated with doming (e.g. Baljinnyam *et al.* 1993; Cunningham 2001; Walker *et al.* 2007, 2008). Determining the slip vectors of the normal faults, and hence determining whether they are compatible with the regional strain field, will help to distinguish between the differing scenarios.

Geomorphology of the Egiin Davaa rupture

The Egiin Davaa fault is a prime example of the relatively long NE–SW-trending normal faults that cut through the highest elevations of the Hangay Mountains (Figs 1 & 2). Elevations in the uplifted southeastern side of the fault reach *c.* 3500 m. The valley of the Badraig Gol (Badraig River) runs along the immediate hanging wall. The fault trace itself is situated at elevations of *c.* 2000–2500 m. Although there is relief of >1 km across the fault, the major part of this relief is due to fluvial incision into the dome-shaped Hangay Mountains (e.g. West *et al.* 2013) and the cumulative vertical displacement across the Egiin Davaa fault is <250 m. The geomorphology along the northeastern part of the fault is dominated by glacial or periglacial landforms. The landscape gradually changes to open steppe to the SW.

A semi-continuous scarp, with a vertical displacement of 4–4.5 m along its entire length, cuts

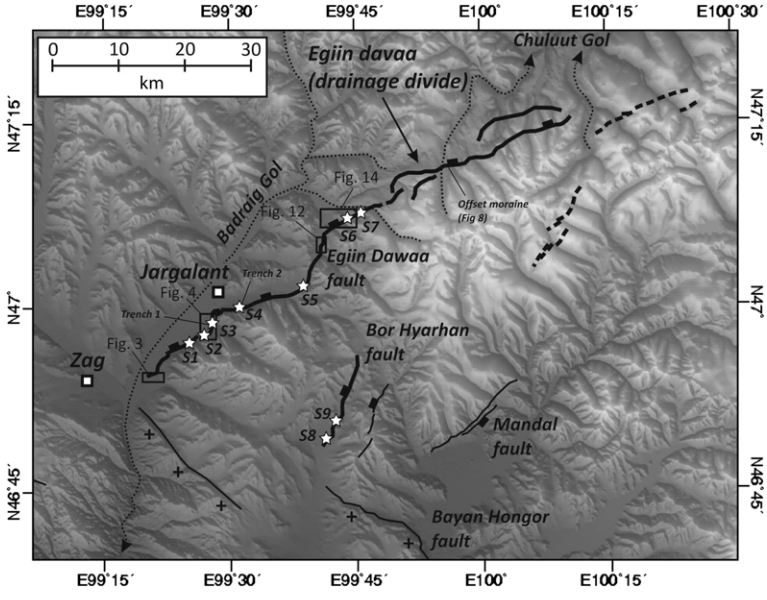

Fig. 2. Shuttle Radar Topography Mission hillshade topography illuminated from the SW. The Egiin Davaa fault forms the drainage divide between tributaries of the south-flowing Badriag Gol and the north-flowing Chuluut Gol. The Egiin Davaa and Bor Hyarhan palaeo-earthquake ruptures are marked with thick black lines. Potential continuations of the Egiin Davaa rupture in the high mountains which we have not confirmed in the field are represented by thick dashed lines. Other faults with evidence of late Quaternary movement are drawn with the upthrown sides marked with + symbols. The nine scarp profile measurement sites are marked by white stars. The black boxes represent the regions shown in later figures. This map is in a Mercator projection.

across and displaces late Quaternary alluvial and glacial deposits along the southeastern side of the Egiin Davaa pass (Natsag-Yum *et al.* 1971; Khil'ko *et al.* 1985; Baljinnyam *et al.* 1993; Schlupp 1996; Cunningham 2001). Along its length, the scarp shows en echelon segmentation at the 100 m scale, with typical steps between individual segments of 10–20 m, along with a few larger steps of *c.* 100 m width at which small pull-apart features have formed. This small-scale segmentation is likely to be superficial and probably does not reflect segmentation of the fault at depth. The only larger scale discontinuity in the fault trace is found immediately west of the Egiin Davaa pass, where there is a *c.* 2 km step in the fault trace (Fig. 2). The continuity and steepness of the Egiin Davaa scarp has led to it being interpreted as resulting from a single earthquake. Khil'ko *et al.* (1985) first described the ruptures and assigned an age of 300–500 years based only on the apparent freshness of the ruptures. Baljinnyam *et al.* (1993), Schlupp (1996) and Cunningham (2001) provide additional descriptions of the Egiin Davaa fault and rupture.

The rupture is very easy to see along its entire *c.* 80 km length, both in satellite images (e.g. Figs 3 & 4) and in the field (Figs 5–8). The southern part of the rupture (the part roughly between the villages of Zag and Jagalant; Fig. 2) cuts across a broad low-relief alluvial plain on the SE margin of the Badraig Gol. This region is historically significant as the site where Temudjin (the future Chinggis Khaan) defeated his rival Jamuha. Near this location, the strike of the fault changes abruptly between sections striking almost north–south and others where the strike approaches east–west.

KOMPSAT-2 satellite imagery of the SW end of the mapped scarp, along with an interpretation of the geomorphology, is shown in Figure 3. Here, the fault trends WSW–ENE and cuts the surfaces of a series of coalescing alluvial fans (highlighted in dark orange in the interpreted image; Fig. 3) originating from small catchments in hills to the south. A right-stepping arrangement of en echelon fault segments towards the western end of the image is suggestive of a left-lateral slip component (cf. Baljinnyam *et al.* 1993). In addition, two small basins are present between the overlapping ends of the more widely separated segments in the eastern part of the image, which may result from localized extension at extensional jogs in the fault trace. The alluvial surface has been incised on its upthrown (southern) side by stream channels (beige on the interpretation). Small active fans have formed at the outflow of the incised channels on the northern (downthrown) side of the fault.

At the bottom left-hand corner of Figure 3, the Egiin Davaa scarp crosses a riser between the alluvial fan surface and the floodplain of the Badraig Gol (shown in gold on the interpretation). South of where the scarp enters the river floodplain, a single terrace is preserved at an elevation between the fan surface and the present floodplain. The surface of this terrace, which is shown in detail in the inset image in Figure 3, is covered in boulders and preserves remnants of meandering channels of a form very similar to that of the present floodplain. As the terrace is only present south of the Egiin Davaa fault, we infer that it represents uplift of the floodplain of the Badraig Gol. Because there is only a single terrace, despite it being in the floodplain of a large river, this provides confirmation that the scarp was formed in a single earthquake. Alternatively, if the scarp had formed in multiple earthquakes, then we would expect to see fragments of multiple terraces in the margin of the river floodplain. The maximum scarp height in this section of the fault is *c.* 4.5 m (all profile measurement sites are marked by white stars in Fig. 2 and are labelled S1–S7). Each 'site' consists of multiple individual scarp profiles collected within *c.* 100 m of each other to give a measure of the small-scale variability in scarp height caused by 100 m-scale segmentation. The profile heights for each site along the entire rupture length are plotted in Fig. 9 and individual profile analyses are presented in the Appendix.

Figure 4 shows KOMPSAT-2 imagery of the transition from the WSW–ENE-trending fault segment described in the preceding paragraph (and shown in Fig. 3) to a north–south trend. The scarp is segmented, but in the north–south section there appears to be a left-stepping en echelon arrangement of 100 m-scale segments suggestive of a component of right-lateral strike-slip. The fault in the region shown in Figure 4 cuts across a coalesced alluvial fan surface. Near the north end of the image a small stream has incised for a distance of *c.* 300 m upstream of the scarp, where a prominent knickpoint is observed. A field photograph of the scarp where it is incised by the stream is shown in Figure 5a. The photograph shows the location of a palaeoseismic trench, which we excavated into the northern margin of the incised stream. Figure 5b shows four topographic profiles measured orthogonal to the scarp in this approximate location. The scarp height is variable between individual profiles, as it was at all measured sites along the fault. The variation in scarp height over distances of tens of metres is likely to result from the small-scale segmentation of the fault trace, which, in turn, may relate to the presence of a strike-slip component of the slip. The maximum scarp height in this section is *c.* 4 m.

Further to the NE, the fault scarp continues to be clearly visible in alluvial fans along the base of hills to the south (Figs 6 & 7). The maximum scarp height in the section of fault shown in Figure 6 (site S4 on

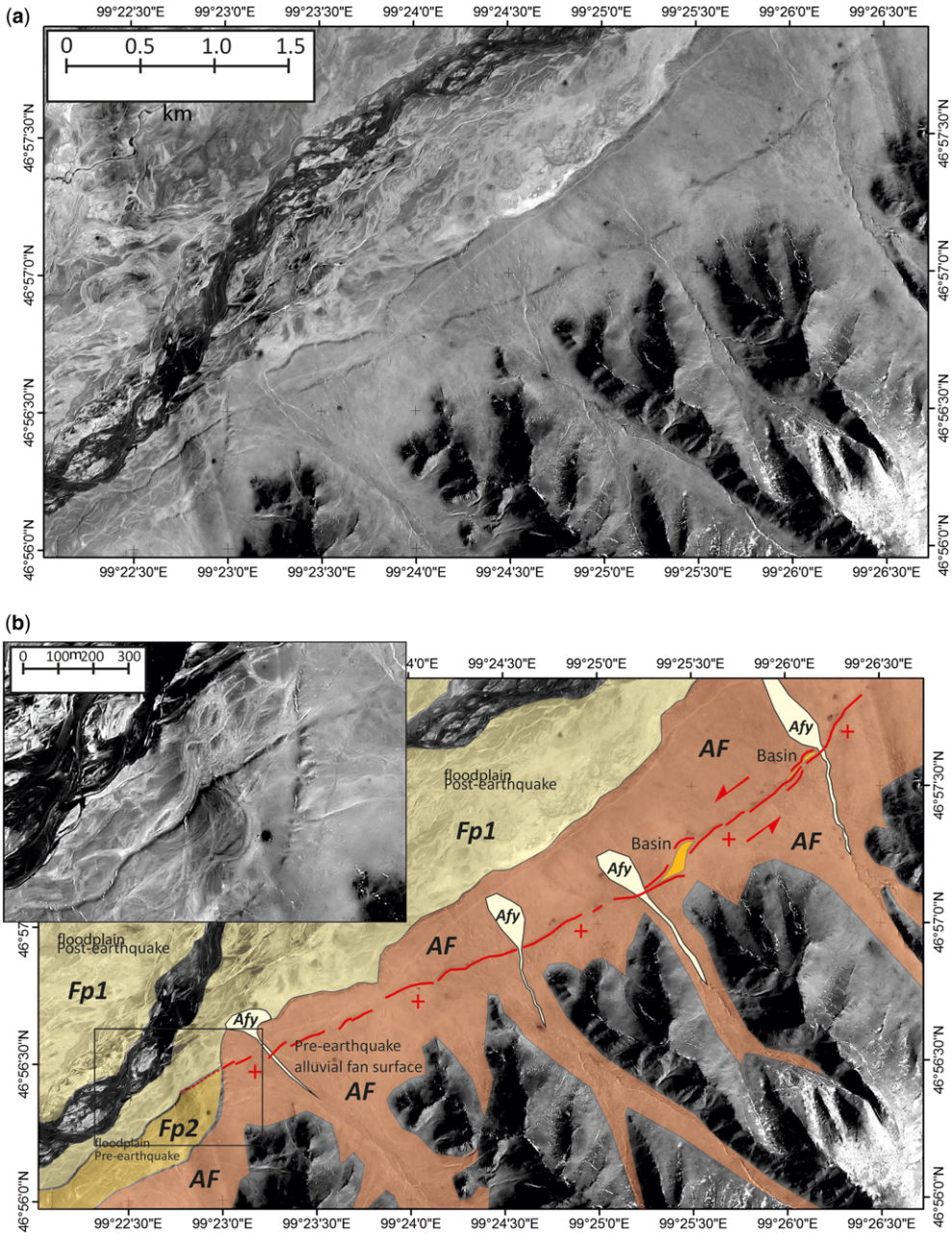

Fig. 3. (**a**) KOMPSAT-2 panchromatic satellite image (1 m pixels) of the SW part of the Egiin Davaa rupture. This image, and all later ones, is in a local zone UTM projection. (**b**) Geomorphological interpretation of the image in part (a). The north-facing rupture (red lines) displaces a series of small coalesced alluvial fans originating from hills to the south (AF). The scarp has been incised by a small number of streams, which form minor alluvial fans on the northern downthrown side of the fault (Afy). At its western end the scarp enters the floodplain of the Badraig Gol (Fp) and has uplifted a portion of the floodplain to form a terrace (Fp2, see inset for a detailed view). The presence of this single terrace is strong evidence for the scarp forming in a single earthquake event and also for very little geomorphological change since that earthquake as there has been little erosion of the upthrown side of the fault by the river. Small pull-apart basins and right-stepping en echelon rupture segments suggest a possible left-lateral component of slip (e.g. Baljinnyam *et al.* 1993).

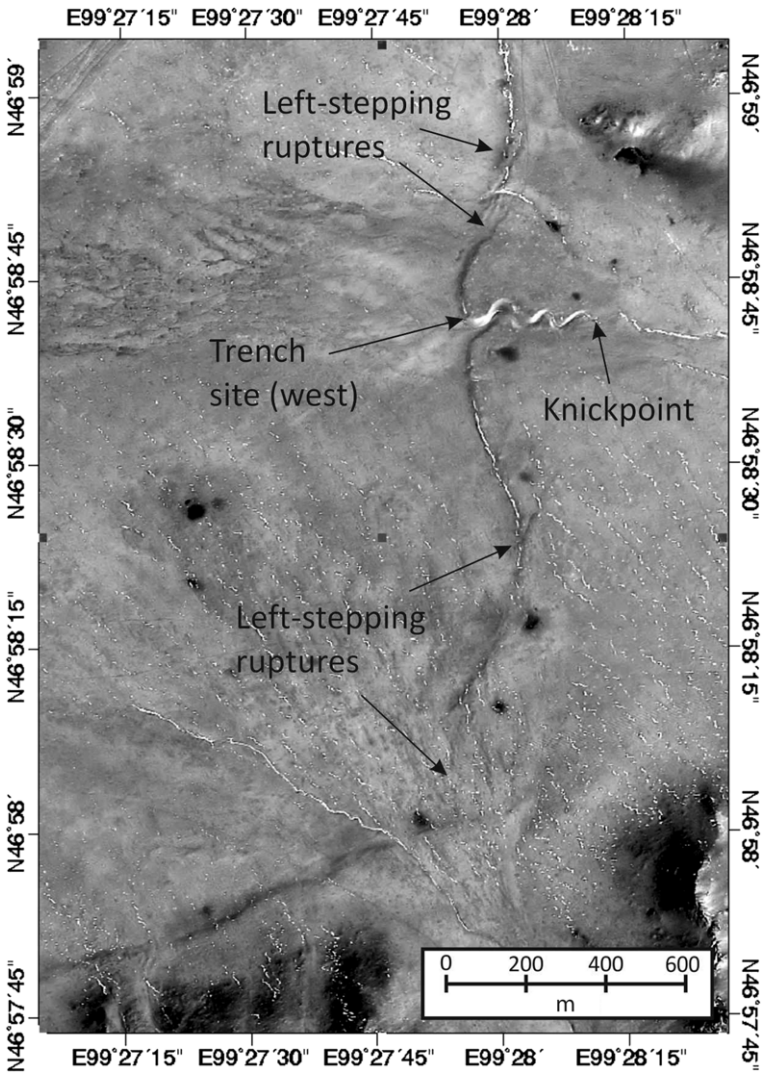

Fig. 4. KOMPSAT-2 panchromatic image of the Egiin Davaa fault where it turns abruptly from east–west to north–south. In the north–south section, the individual rupture segments appear to step to the left, indicating a component of right-lateral slip. Trench 1 (around which we also collected several scarp profiles, collectively referred to as site S3) was dug into the northern bank of an incised stream. The stream incision extends only *c.* 300 m east of the scarp, where there is an abrupt knickpoint.

Fig. 2) is 4.2 m. The northernmost measurements of scarp height were made close to the regions shown in Figure 7. The maximum scarp height at both sites S5 and S7 is *c.* 4.5 m. The measured scarp height at site S6, which is not far from S7 and has a similar strike, is only *c.* 2 m. We suspect that the profiles collected together as site S6 were measured near the end of one of the short en echelon segments and hence the profile measurements from that site are not representative. North of latitude *c.* 47° 05′ N the footwall passes into a region dominated by glacial morphology, with deep U-shaped valleys in the footwall, extensive glacial moraines in the hanging wall and with well-preserved remnants of a pre-uplift erosional surface preserved on the low-relief footwall summit (Figs 3 & 8).

For most of the mapped fault trace, the *c.* 4 m scarp is the only clear indication of late Quaternary slip, but in a few localities we noticed evidence of possible larger late Quaternary displacements representing the cumulative effects of more than one

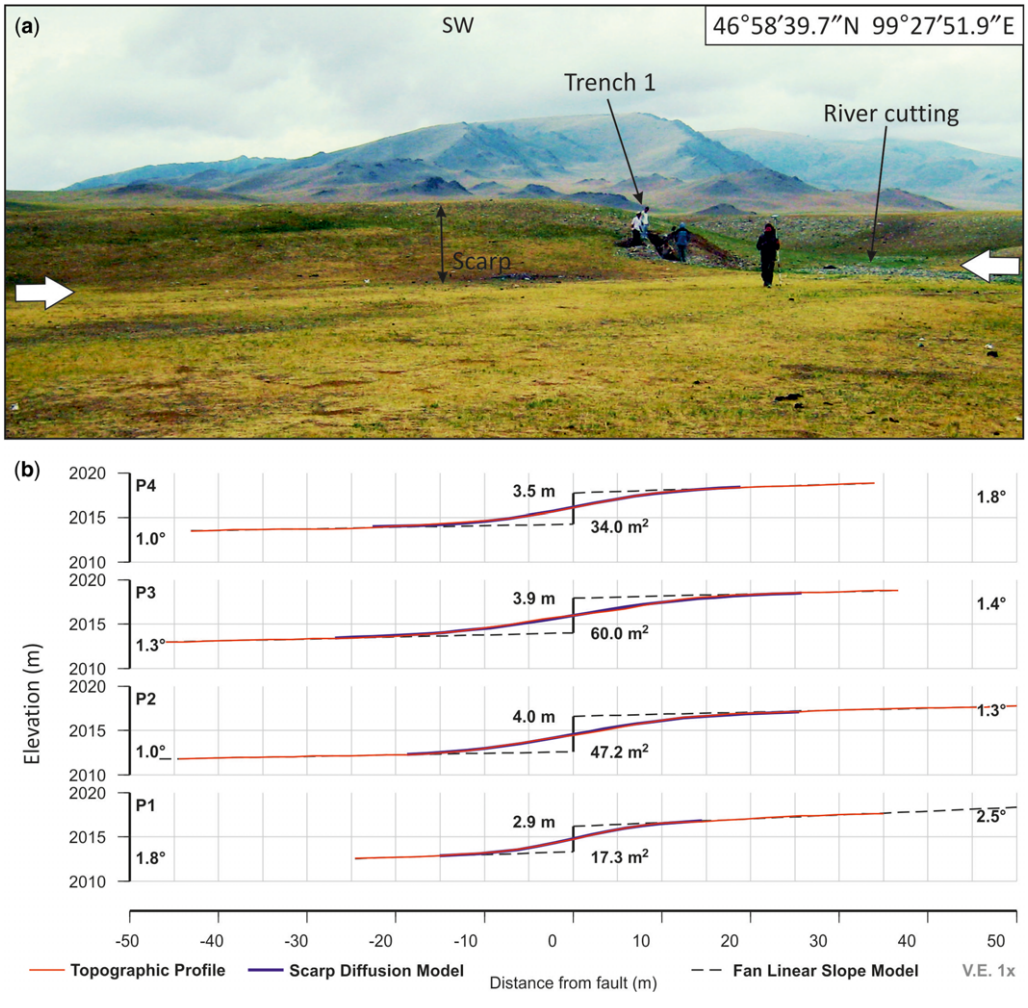

Fig. 5. (**a**) Photograph of the scarp at site S3 (see Fig. 2). The base of the scarp runs between the white arrows. The scarp has a maximum height of 4 m here. A trench (Trench 1) was excavated into the northern bank of a small incised stream. Partially infilled fissures are visible on the scarp. The photographer's location is given in the top-right of the photograph. (**b**) Topographic profiles across the scarp at site S3. The vertical displacement is given in metres and the maximum slope of each is given in degrees. The variability in scarp height between successive closely spaced profiles is likely to reflect the superficial *c.* 100 m-scale segmentation of the rupture. The maximum scarp slope at site S3, averaged from the four profiles, is 11 ± 1°. See Appendix for all other topographic profiles.

earthquake. The most convincing of these is a continuous *c.* 8 m scarp along the northern section of the fault, where it is preserved in Cenozoic volcanic rocks (e.g. Fig. 8). Along this section the fault also offsets a recessional lateral moraine of the Chuluut Gol valley by 8 m (at 47° 11′ 30.72″ N, 99° 57′ 8.1″ E, Fig. 8c). We also found one locality at lower elevations (at 47° 01′ 59.9″ N, 99° 39′ 25.9″ E, not shown in any figure), where possible fragments of an older alluvial fan, at an elevation of *c.* 8 m above the present day river level, are preserved at the margins of an incised river catchment. Adjacent to the Chuluut Gol, the fault offsets late Miocene basalt flows, in places forming two distinct sub-parallel segments, where at least 225 m of fault throw has accumulated since the eruption of the $^{40}Ar/^{39}Ar$ dated capping flow at 6.27 ± 0.16 Ma (Tielke *et al.* 2007; Ancuta *et al.* 2013; Fig. 8a).

Khil'ko *et al.* (1985) estimated an average scarp height of 3.0–3.5 m in the NE and 3.5–4.0 m in the SW. Khil'ko *et al.* (1985) also noted that, in the central section of the fault, the rupture splays into two or three sub-parallel traces, such that the total scarp height might be up to 4.0–4.5 m. Our

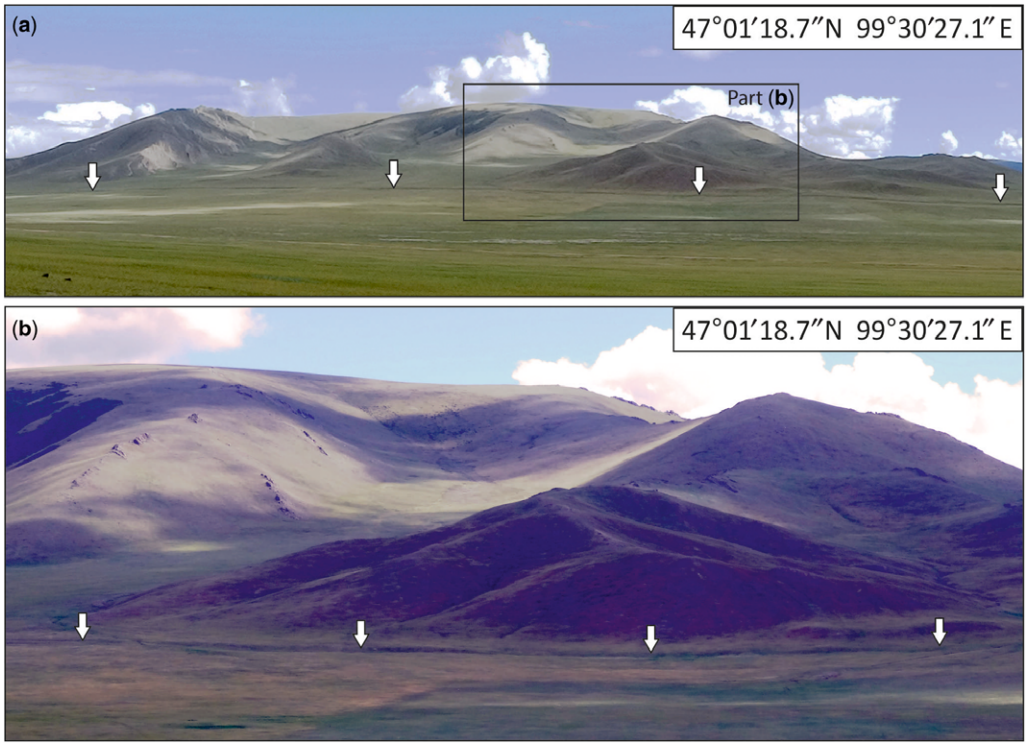

Fig. 6. (**a**) Panoramic photograph showing the continuity of the scarp (marked by white arrows). Topographic profile measurement site S4 is mid-way along this view. Trench 2 was also dug along this section. Much of the relief in the footwall is not related to slip on the fault. (**b**) Close-up showing the scarp, in shadow, tracking along the base of the hills. The photographer's location is given in the top-right of each photograph.

measurements of the scarp height from topographic profiles broadly agreed with these estimates. All scarp profiles are included in the Appendix and the height measurements are plotted as a function of longitude on Figure 9b. We note that, although the local fault strike at our measurement sites varies by *c.* 80°, the maximum scarp height does not vary substantially, being *c.* 4–4.5 m irrespective of either the local strike or of the position along the rupture length.

The Bor Hyarhan rupture

In addition to the *c.* 80 km of rupture described in the preceding section, we identified a second rupture sited *c.* 20 km SE of the main Egiin Davaa fault (Fig. 2). This rupture is *c.* 20 km long with a strike of *c.* 010°. In the perspective view shown in Figure 10, the scarp is visible and runs in front of (west of) a degraded footwall block in bedrock. Several eastwards-flowing drainages have been blocked at the fault, with their old courses preserved as dry valleys in the uplifted footwall (marked by stars on Fig. 10).

We visited the southern part of this scarp in July 2008, and again in July 2013, to make observations in the field (Fig. 11) and to collect several topographic profiles orthogonal to the scarp using kinematic GPS (locations S8 and S9 on Fig. 2; see Appendix). From its southern end, the scarp rapidly increases in height to a maximum of *c.* 2.8 m. It is possible that the scarp increases further in height north of the section investigated in the field. Morphological dating of the scarp, compared with a similar analysis for the main Egiin Davaa scarp, indicates that the two ruptures may have formed at a similar time, possibly due to stress transfer between the two structures, or potentially as subevents of the same earthquake.

Age of the ruptures

In the preceding section we used the geomorphology of the Egiin Davaa scarp to confirm that it resulted from slip in a single earthquake. An additional 20 km of rupture may also have occurred on the Bor Hyarhan fault during that event. The existing age constraints on many of the known

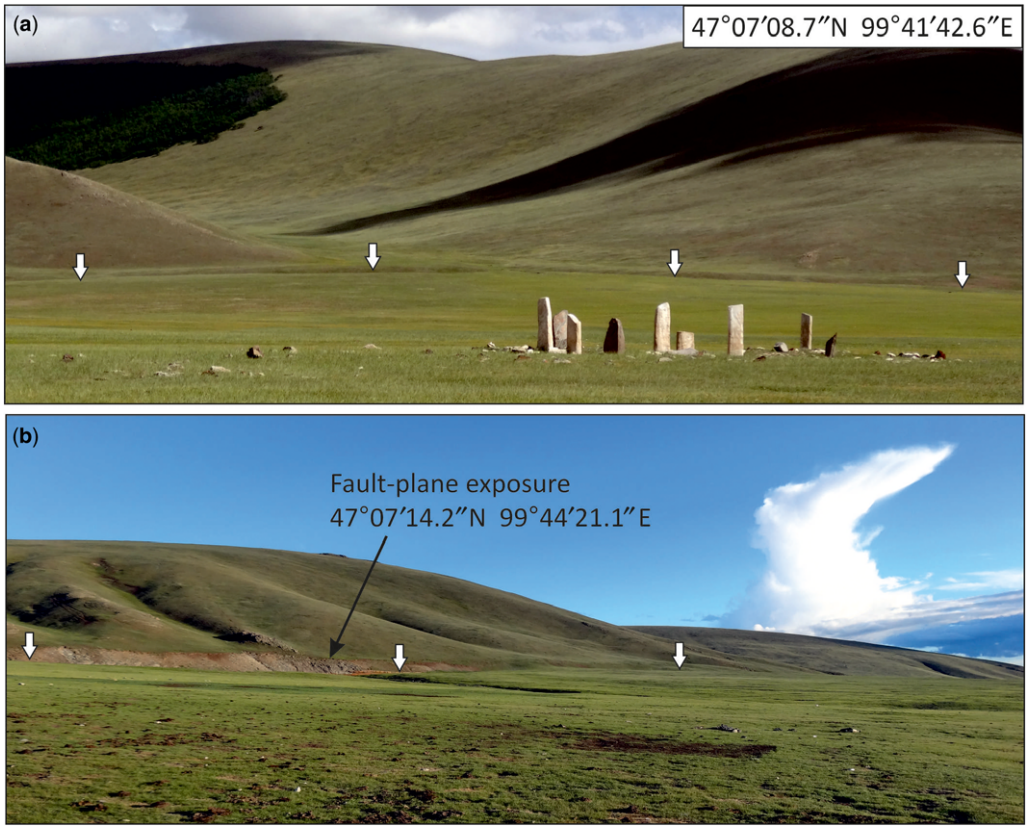

Fig. 7. Field photographs of the Egiin Dawaa scarp mid-way along the 80 km-long rupture. (**a**) The scarp cutting across the apex of a small alluvial fan, with prehistoric standing stones in the foreground. (**b**) The scarp running along the base of low hills in schist bedrock. Towards the left-hand side of the image, spring water emanating from the fault has removed the overlying soil cover and exhumed a fault plane in bedrock (see Fig. 14).

prehistoric earthquake ruptures in Mongolia come from qualitative assessments of their level of preservation compared with other ruptures of known age (e.g. Baljinnyam *et al.* 1993). Using this approach, Khil'ko *et al.* (1985) assigned an age of 300–500 years to the ruptures. Mongolian legends tell of a large magnitude event in this general area during the life of Avday Sayn Haan in the latter half of the sixteenth century (Natsag-Yum *et al.* 1971) and the Egiin Davaa rupture has been interpreted to result from that event.

In the following, we provide new estimates of the age of the Egiin Davaa rupture, both from palaeoseismic trenching and from morphological dating of the fault scarp. The first line of evidence for dating the scarp formation, however, comes from an analysis of satellite imagery. Figure 12 shows a KOMPSAT-2 satellite image of a north–south section of the fault (see Fig. 2 for location). Prehistoric burial mounds (*khirigsuur*), which typically date to 2500–3000 years ago (Allard & Erdenebaatar 2005; Wright 2007), are present at both the top and bottom of the scarp. The two *khirigsuur* at the top of the scarp (labelled 1 and 2) are sited on either side of a stream incised into the scarp. The close proximity of the burial mounds to the scarp and the incision implies that they post-date scarp formation. An age of several thousand years for the Egiin Davaa earthquake is also supported by trenching and morphological dating of the scarp.

Palaeoseismic investigation

We excavated two trenches through the Egiin Davaa fault scarp, one at 46° 58′ 39.7″ N, 99° 27′ 51.9″ E and another at 47° 0′ 25.06″ N, 99° 32′ 45.20″ E, in the summer of 2006. Both were dug by hand. The trench logs are presented in Figure 13. Trench 1 was dug into the side of an incised stream channel (Fig. 5) and so the ground surface shown in the log is

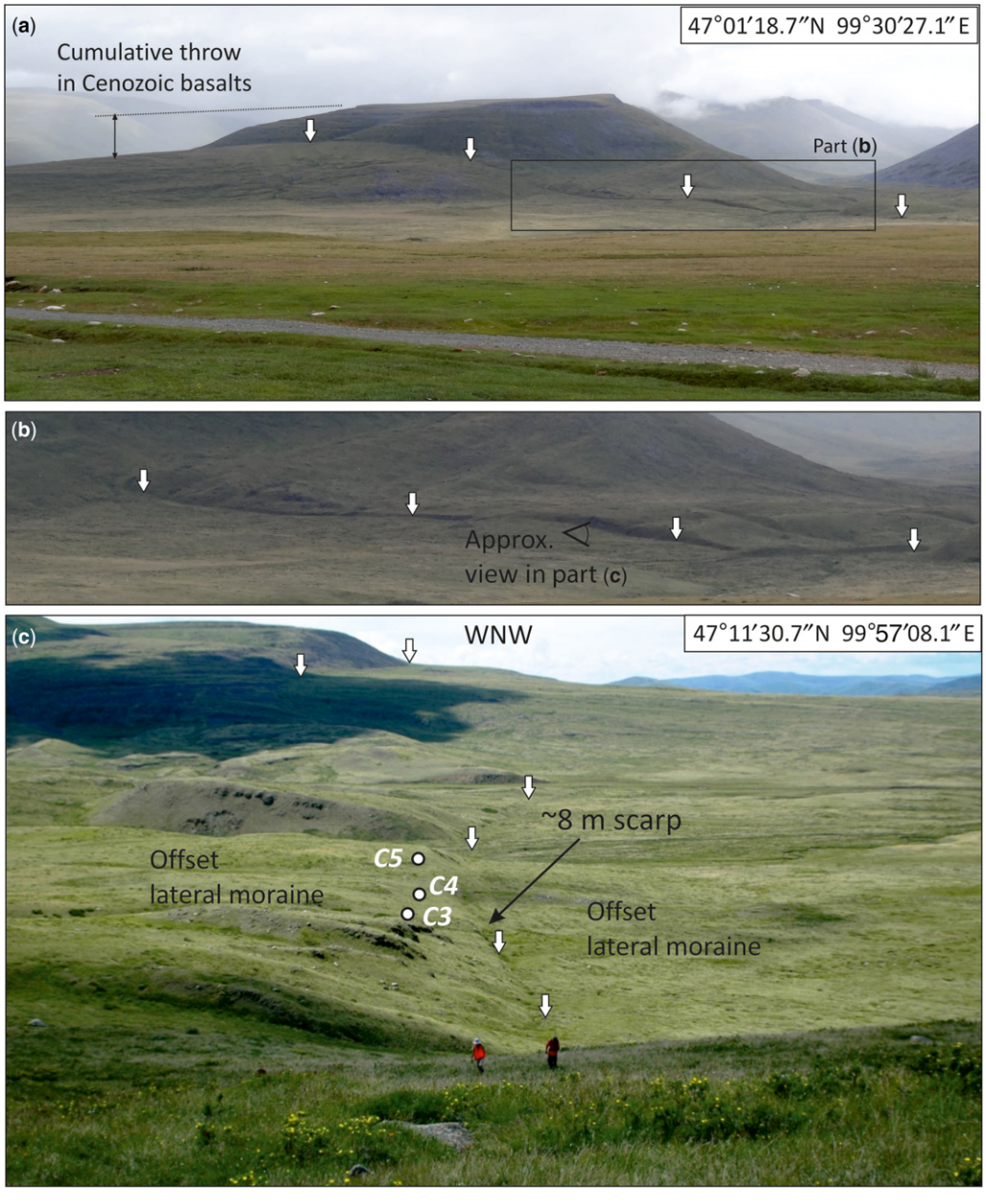

Fig. 8. (**a**) Field photograph looking SE from the roadside at Egiin Davaa pass. The Egiin Davaa fault has displaced the top surface of the Cenozoic lava flows, yielding a maximum Cenozoic throw of 225 m. Towards the right-hand side of the view, the rupture crosses a wide U-shaped valley, where the scarp cuts through a late Quaternary moraine at the margin of the valley, as shown in detail in part (**b**). (**c**) Field photograph looking WNW at the *c.* 8 m high scarp in the moraine. Approximate sites of granite boulder samples C3–5 for cosmogenic ^{10}Be exposure dating (Tables 2 & 3) are shown.

not representative of the general slope of the fault scarp. The general stratigraphy exposed in the walls of Trench 1 was of coarse angular alluvial deposits interrupted by three light-coloured silt horizons containing sparse sub-angular clasts, which we interpret to be palaeosol horizons. The palaeosols

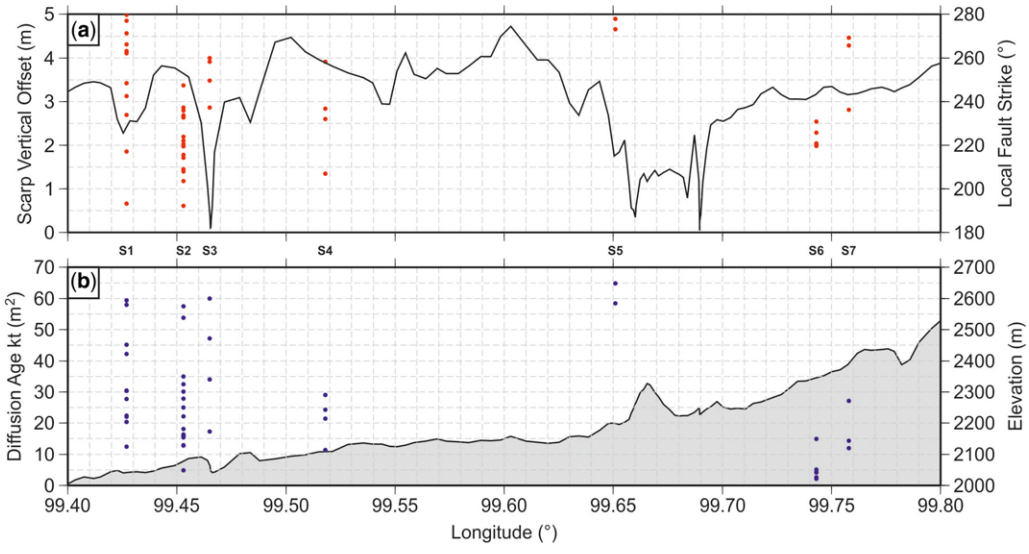

Fig. 9. (**a**) Range of calculated scarp vertical offsets (closed circles) shown as a function of longitude (in decimal degrees). Variability in scarp height at individual strikes is likely to arise from small-scale fault segmentation and stepping between segments, with the maximum at each site likely to represent the true throw (vertical offset). The local strike calculated from the satellite trace of the rupture is denoted by the black line. The bulk of the rupture strikes WSW, but with two segments almost striking due south. (**b**) Range of diffusion ages (closed circles) calculated at the seven sites (S1–S7) SW to NE along the Egiin Davaa fault rupture. The elevation (grey profile) along the fault rupture at the sites measured increases from about 2050 to 2400 m. Diffusion age may decrease at higher elevations.

(labelled P1, P2 and P3 from oldest to youngest) are likely to indicate soil formation during periods of fan surface stabilization, an interpretation supported by the presence of fossil rootlets in P1 and P2. Such periods may represent climatically modulated changes in sediment supply in the fan system, or simply periods of migration of the position of the main channel, and so their development is not necessarily related to fault slip events. The palaeosol layers are *c.* 10 cm thick and presumably formed as relatively planar bodies, but now all show either displacement or warping of the same magnitude consistent with surface rupturing in at least one earthquake post-dating the youngest of the three layers.

Three faults were identified in the trench walls (F1, F2 and F3). We interpret F3 to be the main fault zone. It has a dip of *c.* 60° W in the upper metre of the trench and shallows to a dip of *c.* 35° W below this. Fractures F1 and F2 dip steeply to the east and are antithetic to the main fault zone. F1 displaces the lowest palaeosol horizon (P1) by *c.* 30 cm (down to the east). The middle palaeosol unit (P2) is also deformed by the F1 fault, but by a combination of displacement and warping above the fault tip. The combined amount of displacement and warping in P2 is of a similar magnitude to the displacement of the lowest layer (P1). The uppermost palaeosol unit (P3) is not displaced, but is warped at a point *c.* 1 m north of the projection of the F1 fault. P3 is not preserved on the upthrown side of F1, but the observed warping in P3 is not less than 30 cm. Although we did not identify a discrete dislocation cutting the sediments up to P3, we inferred that the dip of the F1 fracture decreases in the upper part of the stratigraphy and intersects P3 where it is deformed. We inferred that the P3 unit represents the surface unit when F1 ruptured because the living root network may have been sufficiently cohesive to prevent the development of a discrete fault at the surface.

The highest of the palaeosol horizons (P3) is deformed by both the F2 and F3 faults. It has been broken into a number of short fragments and appears to be mixed with alluvium. We interpret the jumbled remnants of palaeosol and alluvium between F2 and F3 to represent colluvium derived from the collapse of the upthrown fault block. The antithetic F2 fracture extends into the P3 horizon. The P3 palaeosol is not preserved on the southeastern, upthrown side of the main fault (F3). This observation suggests that a significant amount of material has been removed from the upthrown block and re-deposited downslope. The pronounced scarp degradation at the trench site is a local effect because the excavation was made into the side of an incised gully.

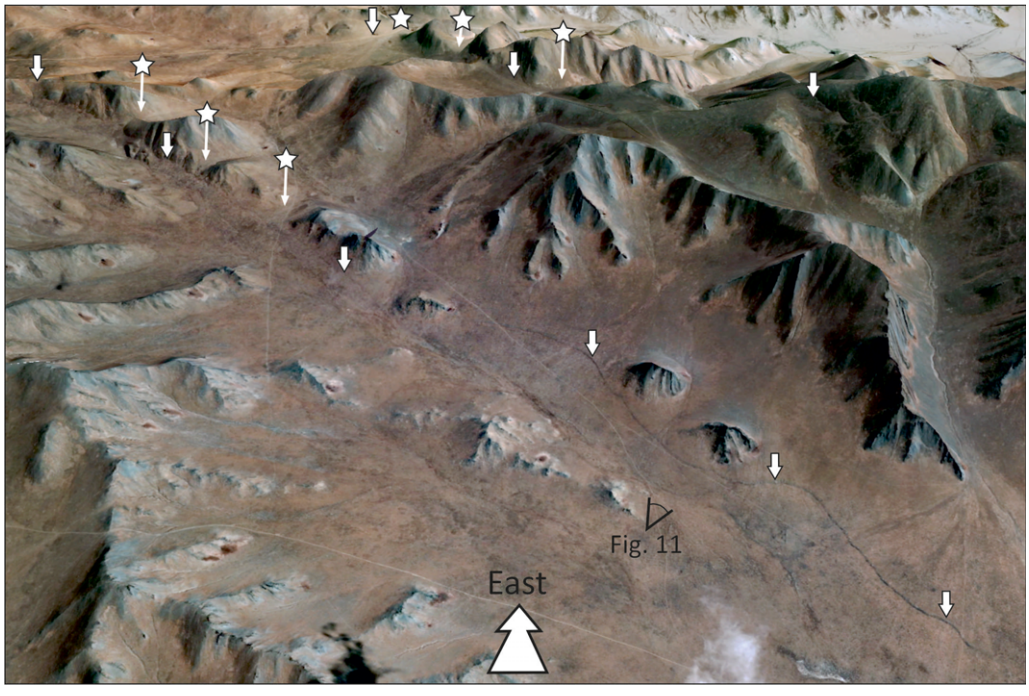

Fig. 10. Oblique view of the Bor Hyarhan scarp. The scarp, in shadow, is marked by a series of white arrows. A series of wind gaps in the uplifted footwall are marked by white stars. The footwall of a third fault is visible in the distance. This third fault does not have a scarp in late Quaternary alluvial material along its base, but is instead identified from a series of triangular facets and wind gaps cut into the schistose bedrock of its footwall.

The most recent soil layer (P4), which is not fractured or deformed by faulting, thickens on the downthrown side of the fault, from which we interpret it as a colluvial wedge post-dating the slip event. The thickest section of the P4 soil is bounded by the opposing faults F1 and F3, which we interpret as the result of infilling of a shallow graben at the surface.

The displacement of the upper parts of the exposed stratigraphy by the three faults (F1–F3) is compatible with movement in a single slip event that post-dates deposition of the P3 palaeosol and predates deposition of the most recent soil layer (P4). None of the palaeosols is preserved on the upthrown side of the fault as exposed in the trench, suggesting that much of the immediate footwall has been eroded. As the palaeosol units are not preserved on the upthrown side of the fault, we are unable to determine the total vertical displacement across the fault zone. We can, however, estimate the minimum throw by assuming that the P1 unit was once located above the present land surface (e.g. Fig. 13a). Therefore we know that the displacement in this earthquake was >2 m.

To provide age constraints on the palaeo-earthquake recognized in the trench we dated the two lowest palaeosols (P1 and P2), using charcoal and fossil rootlets preserved in the soils and extracted from samples collected in 2006, at *c.* 7.6 and 7.4 ka (calibrated radiocarbon age BP, Table 1). These two units are displaced by faulting, which must therefore date to <7.4 ka. Unfortunately, we were unable to isolate fossil organic material within the upper palaeosol units and so only have an upper bound on the age of the scarp-forming event.

Trench 2 was located on the downthrown side of the Egiin Davaa fault at 47° 00′ 25.06″ N, 99° 32′ 45.20″ E (see Fig. 2). The scarp exhibits 2.5 m of relief at the trench site. The trench was 8.5 m long and up to 2 m deep and did not intersect the fault plane. As a result of time constraints, we were not able to lengthen the trench towards the fault. The basal unit in the trench is clast-supported alluvial gravel, which we interpret as predating the last rupture event. We did not observe buried soils in this trench, which we did in Trench 1, suggesting that the alluvial gravels are not much older than the age of the last rupture. A fissure or scarp-parallel graben-fill deposit that consists of massive silty sand, possibly aeolian in origin, is unconformably draped against the alluvial gravels. The silty sand is overlain by non-imbricated cobble-dominated

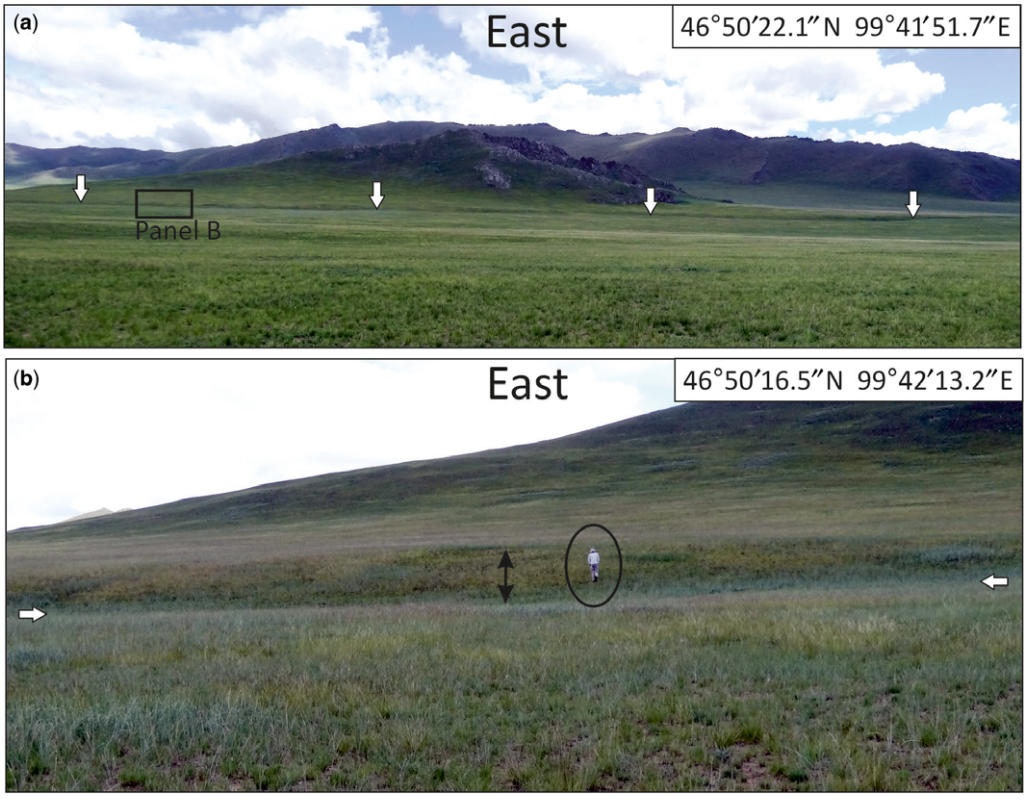

Fig. 11. (**a**) Photograph looking east at the Bor Hyarhan scarp, marked by black arrows, the base of which runs between the white arrows. Bor Hyarhan is the range of low mountains in the footwall. (**b**) Close-up of the Bor Hyarhan scarp (base of the scarp is marked by white arrows, person for scale).

colluvium, probably derived from the adjacent fault scarp. The entire sequence is capped by a 30–50 cm thick cumulic silty sand with a weak modern soil developed in it. We obtained a single radiocarbon age of 4910 $\pm$ 60 years (calibrated radiocarbon age BP) from detrital plant fragments preserved in the massive silty sand of the scarp-parallel graben-fill deposit. Although the graben-fill deposits should provide a limiting minimum age for the last earthquake on the Egiin Davaa fault, the detrital plant remains may have been reworked from levels that predate the earthquake.

Morphological dating of the Egiin Davaa scarp

The continuity of the rupture on satellite imagery and as seen in the field points to a single rupture event. The structural relationships exposed in two palaeoseismic trenches are also compatible with slip in a single event, with a maximum age of 7.4 ka. A minimum age of 3.0–2.5 ka on the scarp comes from its spatial relationship with the *khirigsuur* burial mounds. Below, we use the scarp morphology and its current state of surface degradation to place further limits on the age of this earthquake rupture.

Analysis of the relative elevations of fault scarps cutting poorly consolidated sediments has been widely used to estimate fault rupture ages (Mattson & Bruhn 2001; Phillips *et al.* 2003; Spelz *et al.* 2008; Hilley *et al.* 2010; Koehler & Wesnousky 2011). Normal fault scarps of the Basin and Range Province in the USA were noted to have gentler slopes on older scarps than on those resulting from more recent events (Wallace 1977). Quantitative analysis of scarp degradation as a diffusive process has been used as a method of morphological dating of faulting (e.g. Bucknam & Anderson 1979; Colman & Watson 1983; Andrews & Hanks 1985; Hanks & Andrews 1989; Avouac 1993) and has been reviewed by Hanks (2000).

The principle of the technique relies on the fact that a step in topography is smoothed out over time and that the transport of mass downhill is

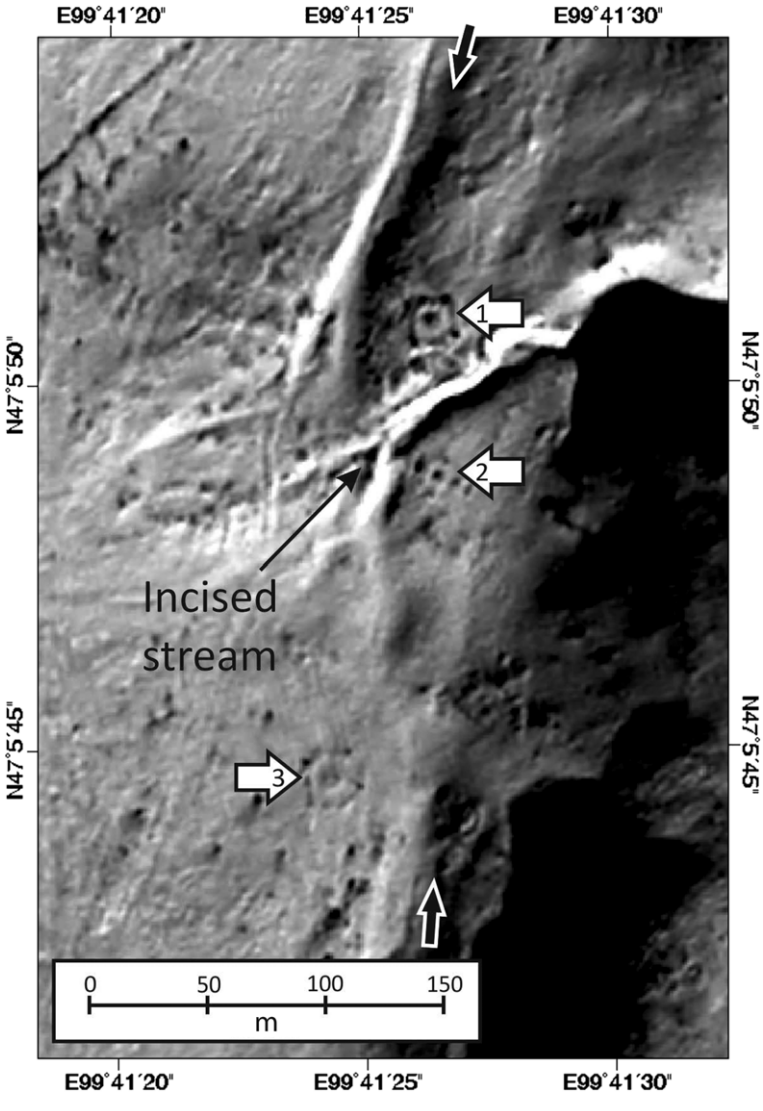

Fig. 12. KOMPSAT-2 panchromatic image (1 m pixels) of the Egiin Davaa scarp (see Fig. 2 for location). The eastern side of the fault, which runs between the black arrows, is upthrown. Three *khirigsuur* grave circles (marked by numbered white arrows) are sited close to the scarp. Graves 1 and 2 are sited on the upthrown side of the fault on either side of a stream incised into the scarp. Grave 3 is at the base of the scarp. All the *khirigsuur* are very close to the scarp, and to the incised stream, indicating that both the scarp and the incision existed when the burial mounds were constructed. The grave circles are up to *c.* 3000 years old (Allard & Erdenebaatar 2005; Wright 2007), placing a minimum age on the scarp.

proportional to the slope and the mass diffusivity (κ). Analysis of elevation profiles can be used to estimate the product of the mass diffusivity and time since the onset of diffusive degradation of the scarp (t). Therefore the relative succession of fault scarps in a region can be established and, if the mass diffusivity is known, then an age of the scarps may also be determined. Conversely, if the age of rupture is constrained from some other dating technique, then an estimate of the mass diffusivity for the locality can be made.

We used multiple surface topographic profiles across the fault scarp at seven locations along the rupture (Fig. 2, see also Appendix) to estimate a mean diffusion age (κt) for the scarp. The elevation data were collected from fault transects using

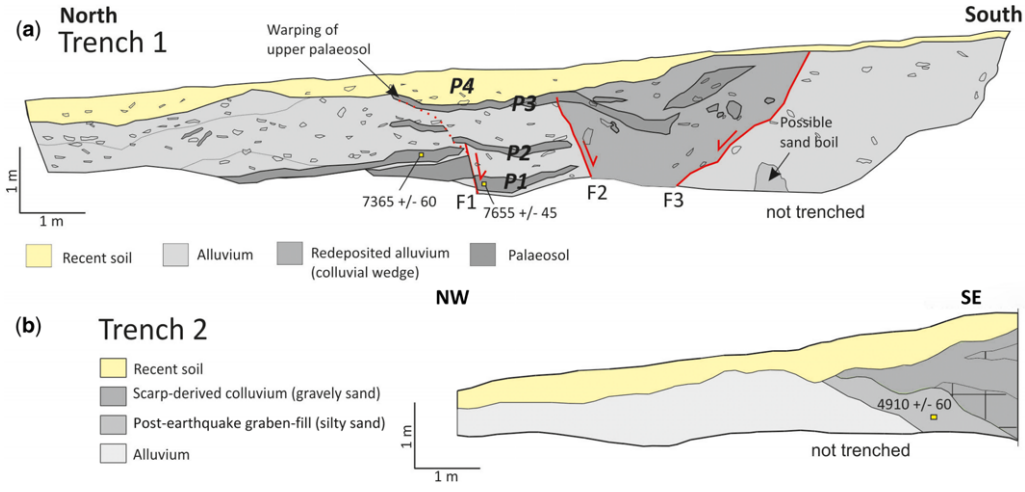

Fig. 13. Log of the stratigraphy exposed in the two trenches. See Figure 2 for approximate locations. Trench 1 is also shown in Figure 5. (**a**) Log of Trench 1 – eastern wall. Three faults (F1–F3) are observed, of which two (F1 and F2) are antithetic to the main fault (F3). An inferred continuation of fault F1 towards a zone of warping in palaeosol P3 is shown as a red dotted line. Three palaeosol units are deformed by the faults. The last movement is hence younger than 7365 $\pm$ 60 calibrated radiocarbon years BP. (**b**) Log of Trench 2 – eastern wall. This short trench did not intersect with the fault plane. We interpret the thick accumulation of silty sand, overlain by a wedge of colluvial material, to result from post-earthquake fissure-fill and scarp diffusion. An age of 4910 $\pm$ 60 calibrated radiocarbon years BP was obtained from detrital plant remains in the basal part of the silty sand. Although the deposition of this unit should post-date the slip event, we cannot exclude the possibility that the detrital remains used for dating are reworked from older, pre-earthquake units.

differential GPS. The fault offset and fan slopes were estimated from points along the profile away from the scarp. These values were then used to constrain the estimates for the diffusion age (κt) using the finite-slope diffusion equation (Andrews & Hanks 1985; Hanks & Andrews 1989) and the near-field scarp profile. A detailed description of our methods is given in the Appendix.

The 46 fault offsets measured at the seven sample sites ranged from 0.7 to 4.7 m, with a mean of 2.8 m. The results for the diffusion age (κt) are given in the Appendix. The mean diffusion age for the 46 profiles at the seven sites along the rupture is 27 m^2 with a standard error in this mean of 3 m^2. Taking the range of mean diffusivity ages (24–30 m^2) found here and combining this with diffusivity estimates for poorly consolidated surficial deposits in the Gobi–Altay of southern Mongolia, the Dzungarian Basin and the Tarim Basin of China (Avouac 1993; Avouac & Peltzer 1993; Hanks 2000; Carretier *et al.* 2002) of 2.3–7.5 $m^2\ ka^{-1}$, and assuming they are applicable to this region of Mongolia, would give an age range estimate for the onset of scarp degradation of 12–4 ka. Taking into account that there is also an initial period of time for a fault scarp to disintegrate to the angle of repose by non-diffusive processes, which may be of the order of centuries (Wallace 1977; Zhang *et al.* 1986), the minimum age of the faulting constrained by diffusion modelling is 4 ka. A minimum age of 4 ka is compatible with our interpretation that the scarp formation predates construction of *khirigsuur* burial mounds (Fig. 12), which are 2500–3000 years old. For the rupture to be 300–500 years old (Khil'ko *et al.* 1985) would require a high rapid diffusivity of 40 $m^2\ ka^{-1}$ based on the mean diffusion ages found here. This high diffusivity is four times larger than any found for a range of locations by Hanks (2000) and therefore very unlikely given Mongolia's cold and arid climate.

If we make the assumption that the single detrital radiocarbon age of *c.* 4.9 ka extracted from the post-event sediments in Trench 2 represents the approximate age of the earthquake, we can estimate a diffusivity constant based on the mean diffusivity age (24 $\pm$ 3 m^2) of 4.9 $\pm$ 0.5 $m^2\ ka^{-1}$, a value similar to that found in the compilation by Hanks (2000) for western China and two to five times greater than those estimated from the Basin and Range Province in the USA.

The eight profiles from the Bor Hyarhan rupture at 99.70° E, 46.82° N (Fig. 2 and Appendix) are not amalgamated with the other 46 profiles in the

Table 1. *Radiocarbon concentrations are given as fractions of the modern standard, $\delta^{14}C$, and conventional radiocarbon age, following the conventions of Stuiver & Polach (1977)*

Lab ID*	Trench	Material dated	$\delta^{13}C$ (‰)	Modern fraction	$\delta^{14}C$ (‰)	^{14}C age (BP)	Calibrated† 2σ age (BP)	Calibrated‡ 2σ age
UCIAMS-27786	1	Charcoal	-23.2 ± 0.1	0.4495 ± 0.0009	-550.5 ± 0.9	6425 ± 20	7365 ± 60	5480–5350 BC
UCIAMS-29775	1	Plant detritus	-23.6 ± 0.1	0.4267 ± 0.0011	-573.3 ± 1.1	6840 ± 20	7655 ± 45	5750–5660 BC
UCIAMS-29776	2	Plant detritus	-24.7 ± 0.1	0.5813 ± 0.0014	-418.7 ± 1.4	4355 ± 20	4910 ± 60	3020–2900 BC

Data are quoted as mean $\pm$ SD values.

*Analyses performed in August 2006 at the University of California Irvine Keck Carbon Cycle AMS Facility. Sample preparation backgrounds have been subtracted based on measurements of ^{14}C-free coal. All results have been corrected for isotopic fractionation according to the conventions of Stuiver & Polach (1977) with $\delta^{13}C$ values measured on prepared graphite using the AMS spectrometer. These can differ from the $\delta^{13}C$ of the original material if fractionation occurred during sample graphitization or the AMS measurement.

†Radiocarbon age determinations were calibrated with the OxCal online calculator, version 4.2.3 (Ramsey & Lee 2013), using the IntCal13 atmospheric curve (Reimer *et al.* 2013).

‡Calibrated ages are rounded to the nearest decade.

calculation of the mean diffusion age because they occur on a structurally separate rupture. However, this southern rupture has estimated offsets in the range 1.5–3 m and diffusivity age values in the range 15–57 m^2, which is within the bounds found for the Egiin Davaa rupture. The mean and standard error values are 30 ± 5 m^2, overlapping within error with the main rupture diffusion age of 24 ± 3 m^2.

Slip direction

Fault plane exposures in bedrock occur at several locations along the Egiin Davaa fault. A fault plane in fractured quartzite bedrock is exposed at 47° 07′ 18″ N, 99° 44′ 27″ E, where spring water emanating from the scarp has removed the overlying soil and colluvium (Cunningham 2001; Figs 7b & 14). The exposed fault plane has a strike of *c.* 075° and a dip of *c.* 35° NNW. Striations show a slip-vector azimuth of *c.* 030°, indicating a large right-lateral component of slip (Cunningham 2001). This right-lateral component is at odds with the right-stepping arrangement of the rupture segments noted by Baljinnyam *et al.* (1993) and the possible left-lateral offsets noted where the rupture crosses incised rivers (Schlupp 1996). A slip-vector azimuth of *c.* 030° would also result in almost pure right-lateral strike-slip on the sections of the fault that trend close to north–south; however, we know from the topographic profiles across the fault that the scarp height is similar on both north–south- and ENE–WSW-trending sections (e.g. Fig. 9).

A potential explanation for these contradictions is that the striations relate to a geologically earlier period of activity. During our field visit we observed a series of subtle corrugations on the fault surface with an azimuth of 300° (Fig. 14). If the corrugations, rather than the striations, indicate the present direction of slip, then this would lead to a slight left-lateral slip component at the measurement site in addition to extension. A slip vector of 300° would result in similar, although not identical, amounts of extension on both fault trends, with a small left-lateral component on the sections trending ENE–WSW and a slight right-lateral component on those trending north–south. These strike-slip components are compatible with the arrangement of en echelon segments observed on east–west- and north–south-trending sections of the fault (e.g. Figs 3 & 4). Support for a slip vector of 300° comes from an observation by Baljinnyam *et al.* (1993), who refer to a fault plane exposure with striations indicating a slip-vector azimuth of 330–340°. They do not give a precise location of this site, but they describe the striations as being on a surface composed of Neogene basalt, which would place it near the northern end of the rupture at roughly *c.* 47° 12′ N, 100° 00′ E (e.g. Fig. 2). A slip-vector azimuth of *c.* 300° is consistent with a strain field dominated

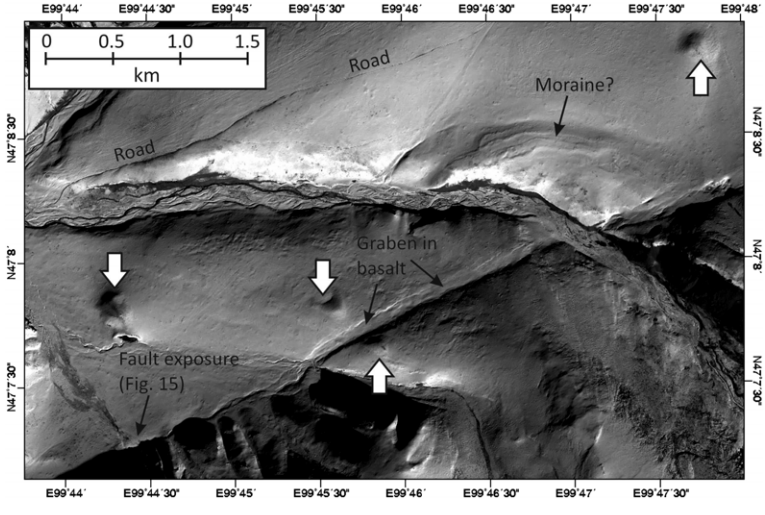

Fig. 14. KOMPSAT-2 panchromatic image of the fault scarp close to the Egiin Davaa drainage divide, at the transition from schistose bedrock exposure (lower left) to Cenozoic volcanics. Topographic profile sites S6 and S7 are located adjacent to Palaeozoic schistose basement in the footwall. Northeast of this image, the scarp is exposed in Tertiary basalt flows and in glacial moraines. The fault exposure and springs shown in Figures 7b and 15 are in the lower left of the image. Quaternary cinder cones are marked by white arrows.

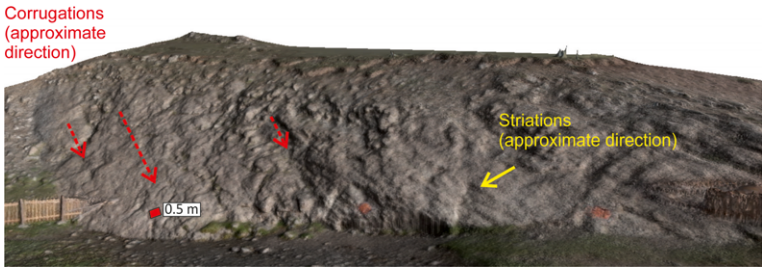

Fig. 15. Three-dimensional model of the exhumed fault plane shown in Figure 7b. The model was produced from multiple photographs taken in the field and combined using the 'structure from motion' method (Westoby *et al.* 2012). Scale is provided by three square markers, each with edge lengths of 0.5 m. One of the markers has been highlighted. Striations on the fault plane observed by Cunningham (2001) approximately follow the arrow on the right-hand side of the photograph. Vague corrugations in the fault surface follow the arrow on the left-hand side of the image. The corrugations point in a direction *c.* 90° from the striations and their existence has implications for the kinematics of faulting.

by east–west left-lateral faulting within central Mongolia (e.g. Fig. 2).

Magnitude

The mapped length of the Egiin Davaa rupture is *c.* 80 km (Fig. 2). The maximum vertical displacement is *c.* 4.5 m and, if the dip of 35°, which we measured from the main fault within Trench 1 (Fig. 11) and from an exposed fault plane in Figure 15, is representative, the maximum slip on the fault plane at the surface approaches 8 m. Applying the scaling relationship between M_w (moment-magnitude) and fault length yields an M_w of 7.3 (Wells & Coppersmith 1994). Using the maximum slip of *c.* 8 m yields a similar value of 7.25. Considering that the scarp height is similar along most of the length of the rupture, we also use 8 m as the average slip, yielding a slightly larger magnitude of 7.4.

We calculate seismic moment (M_o) using the relationship $M_o = \mu Au$ (where μ is the modulus of rigidity, A is the area of rupture and u is the average slip on the fault plane). We have taken the average slip to be 8 m as the scarp height is relatively uniform along much of its length. The area of rupture is calculated from the fault length of 80 km, dip 35°, typical values in Mongolia of 20 km for the seismogenic thickness and 3×10^{10} Pa for the modulus of rigidity (e.g. Bayasgalan *et al.* 2005). We then converted this to a moment-magnitude (M_w) of 7.7 for a fault length of 80 km.

The Bor Hyarhan rupture is *c.* 20 km in length and has a maximum observed scarp height of 2.8 m. We have no direct constraint on the dip of the Bor Hyarhan fault, so we assume a fault dip of 45°, giving a slip on the fault plane of *c.* 4 m. Applying the Wells & Coppersmith (1994) scaling relationship between magnitude and maximum displacement yields a magnitude of *c.* 7 for the Bor Hyarhan rupture.

Long-term slip rate and fault initiation

The geomorphology of the Egiin Davaa fault reveals evidence for only one Holocene surface-rupturing earthquake event along most of its length. There are, however, a few places where late Quaternary cumulative displacements are preserved. These sites allow some limits to be placed on the recurrence interval and average fault slip rate.

Today, the high terrain on the footwall side of the Egiin Davaa fault contains no permanent snowfield or glacier; however, during the late Pleistocene predominantly north-flowing valley glaciers crossed the trace of the fault near Egiin Davaa. Older moraines can be distinguished from younger moraines based on surface boulder frequency, boulder height and hillslope gradient. In one valley immediately north of the main Egiin Davaa divide, a recessional moraine has been displaced by slip on the fault (Fig. 2). The recessional moraine is *c.* 11 km down-valley from the cirques and *c.* 15 km up-valley from the terminal Last Glacial Maximum ice position. At this location, the moraine is offset by 8 m across the fault, probably indicating at least two rupture events since the time of moraine deposition. We obtained cosmogenic ^{10}Be surface exposure ages from three granitic boulders from a post-Last Glacial Maximum recessional lateral moraine (at 2550 m elevation) offset by the Egiin Davaa fault (Fig. 8c; Table 2). The boulders yielded surface exposure ages of 16.2 ± 1.8, 17.6 ± 2.0 and 56.2 ± 5.5 ka. The older age of 56.2 ka is not

Table 2. *Analytical results of terrestrial cosmogenic nuclide ^{10}Be geochronology from the Chuluut Gol recessional moraine*

Sample name	Latitude	Longitude	Elevation (m)	Thickness (cm)[1]	Production rate		Shielding factor	Denudation rate (mm a^{-1})	Quartz (g)[4]	Be carrier (mg)	^{10}Be/^{9}Be ($\times 10^{-13}$)[5,6]	^{10}Be conc. (10^5 at g^{-1} SiO_2)[6–8]	Age (ka)[6,9,10]
					Spallation (at g^{-1} a^{-1})[2]	Muons (at g^{-1} a^{-1})[3]							
C3	47° 11′ 31.74″ N	99° 57′ 15.48″ E	2579	5	33.04	0.412	0.997	0.001	31.1441	0.2987	9.913 ± 0.710	6.384 ± 0.453	17.6 ± 2.0
C4	47° 11′ 30.72″ N	99° 57′ 08.10″ E	2569	5	32.88	0.410	0.999	0.001	33.8927	0.2978	33.143 ± 1.067	19.492 ± 0.626	56.2 ± 5.5
C5	47° 11′ 30.18″ N	99° 56′ 59.82″ E	2560	5	32.68	0.409	0.999	0.001	7.8971	0.2980	2.261 ± 0.167	5.820 ± 0.398	16.2 ± 1.8

The tops of all samples were exposed at the surface.
[1]A constant (time-invariant) local production rate based on Lal (1991) and Stone (2000) was used.
[2]A sea-level, high-latitude value of 4.8 at ^{10}Be per g quartz was used.
[3]Constant (time-invariant) local production rate based on Heisinger *et al.* (2002*a*, *b*).
[4]A density of 2.7 g cm^{-3} was used based on the quartzite composition of the surface samples.
[5]Isotope ratios were normalized to ^{10}Be standards prepared by Nishiizumi *et al.* (2007) with a value of 2.85×10^{12} and using a ^{10}Be half-life of 1.36×10^{6} years.
[6]Uncertainties are reported at the 1σ confidence level.
[7]A mean blank value of 53 540 ± 10 845 ^{10}Be atoms (^{10}Be/^{9}Be = $2.994 \times 10^{-15} \pm 6.03 \times 10^{-16}$) was used to correct for background.
[8]Propagated uncertainties include error in the blank, carrier mass (1%) and counting statistics.
[9]Propagated error in the model ages include a 6% uncertainty in the production rate of ^{10}Be and a 4% uncertainty in the ^{10}Be decay constant.
[10]Beryllium-10 model ages were calculated with the CRONUS-Earth online calculator (Balco *et al.* 2008) Version 2.2 (http://hess.ess.washington.edu/).

Table 3. *^{10}Be ages based on different production rate models*

Sample	Constant production rate		Time-varying production rate models		
	Lal (1991) Stone (2000)	Desilets and Zreda (2003) Desilets *et al.* (2006)	Dunai (2001)	Lifton *et al.* (2005)	Lal (1991) Stone (2000)
C3	17.6 ± 2.0	17.4 ± 2.4	17.5 ± 2.4	16.8 ± 2.0	17.6 ± 2.0
C4	56.2 ± 5.5	53.6 ± 7.0	53.6 ± 6.9	50.5 ± 5.5	55.1 ± 5.3
C5	16.2 ± 1.8	16.0 ± 2.2	16.2 ± 2.2	15.5 ± 1.9	16.3 ± 1.8

Model ages (ka) were calculated with the CRONUS-Earth online calculator (Balco *et al.* 2008) version 2.2 (http://hess.ess.washington.edu/). Data are quoted as mean ± SD values.

realistic given the regional glacial geomorphology and probably includes pre-deposition inheritance of ^{10}Be. Based on the younger two ^{10}Be ages, the moraine was probably emplaced around 16.2 ± 1.5 ka (Fig. 16).

A limiting constraint on the overall age of the fault, and of the total cumulative throw, comes from the northern part of the fault close to the Egiin Davaa pass, where it displaces Cenozoic basalt flows that predate faulting. Around 250 m of fault throw has accumulated since the eruption of the capping flow, which has an ^{40}Ar/^{39}Ar age of 6.27 ± 0.16 Ma (Tielke *et al.* 2007; Ancuta *et al.* 2013, Fig. 8a).

Discussion

The geomorphology of the Egiin Davaa scarp is consistent with formation in a single surface-rupturing event with M_w 7.2–7.7. One trench excavated across the scarp yields evidence of surface rupturing, from which we are able to provide a maximum age of 7.4 ka for the fault movement. A second small trench did not expose the fault zone itself, but detrital plant remains in graben-fill deposits gave an age of 4.9 ka. Diffusional modelling of scarp profiles provides additional constraint, indicating that the scarp formed at least 4 ka ago, assuming that the diffusion coefficient is similar to that found in other arid and cold continental interiors. Finally, the distribution of *khirigsuur* burial mounds along the fault scarp also gives some circumstantial support to its formation before *c.* 3 ka. It is unlikely that the Egiin Davaa rupture formed in the historical event reported by Khil'ko *et al.* (1985).

The extremely well-preserved geomorphology of the Egiin Davaa rupture provides an opportunity to examine evidence for segmentation at various length scales. Segmentation at a 10–100 m scale is present along much of the rupture, which, from its size and consistent en echelon arrangement, is likely to be superficial and to result from a component of strike-slip motion. Other than this superficial segmentation, however, the rupture appears to be continuous for *c.* 50 km from its southwestern end, with a consistent 4 m high scarp along most of its length (e.g. Fig. 2). The southwestern segment is separated from a second segment of *c.* 30 km length that crosses the Egiin Davaa pass (Fig. 2).

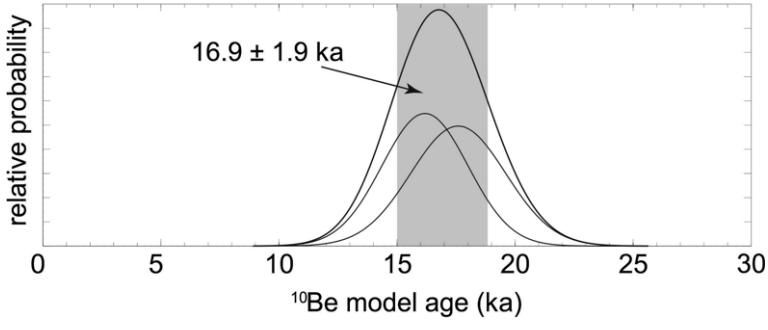

Fig. 16. Probability distribution functions of cosmogenic ^{10}Be ages from two of the three samples collected from the displaced moraine shown in Figure 8c. The third sample yielded an age of *c.* 56.2 ka and was not included in this analysis (see Tables 2 & 3). The combined probability distribution function of the two reasonable boulder ages is shown in black. The one-σ result implies an exposure age of 16.9 ± 1.9 ka.

In general, fault segment length is thought to correlate with the seismogenic thickness of the crust (e.g. Jackson & White 1989; Wallace 1989), with lengths of 20–30 km observed in places where earthquakes occur at depths of *c.* 15 km (e.g. in the Basin and Range Province), whereas fault segments with lengths approaching 100 km are found in regions such as parts of the East African rift, where earthquakes occur at depths of >30 km (e.g. Jackson & Blenkinsop 1997). The continuity of the Egiin Davaa rupture over a distance of at least 50 km may be indicative of relatively large seismogenic thickness, although depths determined for recent earthquakes in the Mongolian region do not typically extend lower than *c.* 20 km (e.g. Bayasgalan *et al.* 2005; Nissen *et al.* 2007).

We interpret 8 m of surface slip due to the shallow dip of the fault where it is exposed. This value is larger than expected from the empirical relationships between slip and length from global earthquakes, which usually have ratios of *c.* 5×10^{-5} (Scholz *et al.* 1986). A fault length of 80 km yields a ratio of 8×10^{-5}. The relatively large amount of slip in large intraplate earthquakes such as that described at Egiin Davaa has implications for seismic hazard assessment within intracontinental regions, as earthquake magnitudes may be substantially larger than those estimated from global earthquake occurrences, the majority of which occur along rapidly deforming plate boundary regions.

We interpret an approximately NW-directed slip vector from fault plane corrugations and from the similar scarp heights for sections of fault trending east–west and north–south. A NW slip-vector azimuth appears consistent with the observed regional pattern of east–west left-lateral faulting (e.g. Fig. 2) and it is likely that reactivation of the Egiin Davaa fault resulted from the regional active tectonics of central Mongolia, rather than as a result of stresses introduced by the locally elevated topography (e.g. Walker *et al.* 2008).

Cenozoic activity on the Egiin Davaa fault is likely to have initiated no more than *c.* 6 myr ago, based on Ar–Ar dating of lava flows that predate fault initiation and are displaced by a maximum of 225 m across the fault. This estimate of total vertical displacement is in agreement with the findings of West *et al.* (2013), who showed that the long-wavelength topography of the Hangay Dome is largely uninterrupted by the mapped active faults. The valley of the Badraig Gol, which is in the immediate hanging wall of the Egiin Davaa fault, is hence likely to be caused by enhanced fluvial incision along the fault, rather than by cumulative fault movement alone. The cumulative displacement of only *c.* 0.3 km is much less than expected from global compilations of fault displacement and length, which predict vertical displacements of several kilometres (e.g. Schlische *et al.* 1996). It is hence likely that the Egiin Davaa fault is an ancient structure that has been reactivated in the late Cenozoic and which has ruptured in two large earthquakes in the last *c.* 16 kyr.

The 225 m displacement of the *c.* 6 Ma basalt flows places a minimum bound of *c.* 0.04 mm a^{-1} on the rate of vertical displacement across the fault. There has been *c.* 8 m of vertical displacement over the last *c.* 16 kyr, yielding an approximate Late Pleistocene vertical rate of *c.* 0.5 mm a^{-1} and an average slip rate of *c.* 1 mm a^{-1}. The full 225 m of vertical displacement could accumulate in a little over 500 kyr at the Late Pleistocene rate. As this rate is calculated from an 8 m scarp that we interpret to result from only two earthquakes, it is unlikely to be accurate and yet does suggest that the late Pleistocene rate is more rapid than that derived from the 6 Ma basalts.

The mismatch between the 6 Ma basalts and late Pleistocene slip rates indicates either that the Egiin Dawaa fault is very young (<1 Ma), or the Late Pleistocene slip is more rapid than the long-term average. Relatively young (*c.* 5 Ma) initiation of faulting has been found in several other deforming parts of Mongolia, including the Gobi–Altay (Vassallo *et al.* 2007) and at the margins of the Altay (e.g. Vassallo 2006). However, variations in slip rate and the clustering of earthquake activity on slow faults in continental interiors is seen in the palaeoseismic record of several regions (e.g. Crone *et al.* 1997) and it is possible that the Egiin Davaa fault has also experienced pulsed activity through the Quaternary. Switching of activity on faults may help to explain the geomorphology of other faults within the Hangay region, such as the Orhon Valley fault (Fig. 1), which have a very clear expression in the large-scale geomorphology, but which show no evidence for rupture in the late Quaternary cover.

Conclusions

We have shown that individual earthquake ruptures in cold, arid continental interiors may be preserved in the landscape for several thousand years. The Egiin Davaa rupture is one of the few palaeoruptures in Mongolia that has been dated, at *c.* 5 ka, and provides an important calibration point for quantifying the linear slope diffusion rate in Mongolia. This study corroborates evidence that many of the presently active faults in Mongolia are relatively young and may relate to a change or reorganization in the kinematics at 5 Ma or younger. There is a suggestion that activity may switch between individual faults, a process that may be widespread in slowly deforming areas, providing another level of complexity in identifying and characterizing potential

sources of future events in such regions. Furthermore, the Egiin Davaa fault represents a rare example of a major earthquake on a reactivated ancient fault, on which there is little Cenozoic cumulative displacement. The fact that such a major earthquake occurred on a fault with little cumulative displacement and relatively low slip rates (probably below the resolution of all but the most long-lived GPS networks) poses a serious challenge for the identification of earthquake hazards. It is only due to the exceptional preservation of fault rupture in this area that this structure has been identified as a potential source of large earthquakes. It remains unclear how much these difficult-to-identify faults contribute to societal risk elsewhere.

The research was funded by the Royal Society of London through a University Research Fellowship awarded to RTW. KW and RC also thank the National Science Foundation (Continental Dynamics Program Award GEO-EAR-1009702) and the Keck Geology Consortium for funding and support. RTW acknowledges support through NCEO/COMET+ and the NERC-ESRC Earthquakes Without Frontiers consortium. The KOMPSAT-2 images were provided through an ESA Category-1 award to RTW. We thank Nathan Toke and an anonymous reviewer for their helpful comments and the editors for compiling this book.

Correction notice: This paper should be published Gold Open Access.

Appendix

We used the linear diffusion method for the degradation of fault scarps to estimate the diffusion age of these features (Hanks 2000). We assumed that a step-like offset in weakly consolidated alluvial fan material relatively quickly degrades to an angle of repose (α) as a result of non-diffusive processes. From then on, the change in the shape of the profile is said to be governed by the following diffusion equation:

$$\frac{\partial u}{\partial t} = \kappa \frac{\partial^2 u}{\partial^2} \tag{A1}$$

Following the results given and same notation as in Andrews & Hanks (1985), the solution to this equation as a function of fault perpendicular distance, x, and time, t, for a single-event scarp having occurred at $x = 0$ in a fan of lower slope β_1 and upper slope β_2, offsetting the surface vertically by amount $2a$ and having already degraded to some assumed angle of repose α at $t = 0$, is:

$$\begin{aligned} u(x,t) = {} & (\alpha-\beta_1)\left[\left(\frac{\kappa t}{\pi}\right)^{1/2}\exp\left(-\frac{(x-x_1)^2}{4\kappa t}\right)+\frac{(x-x_1)}{2}\mathrm{erf}\left(\frac{x-x_1}{(4\kappa t)^{1/2}}\right)\right] \\ & +(\beta_2-\alpha)\left[\left(\frac{\kappa t}{\pi}\right)^{1/2}\exp\left(-\frac{[x-x_2]^2}{4\kappa t}\right)+\frac{(x-x_2)}{2}\mathrm{erf}\left(\frac{x-x_2}{(4\kappa t)^{1/2}}\right)\right] \\ & +\frac{(\beta_1+\beta_2)}{2}x \end{aligned} \tag{A2}$$

where

$$x_1 = \frac{2a}{x-\beta_1+(\alpha-\beta_1)^{1/2}(\alpha-\beta_2)^{1/2}} \tag{A3}$$

$$x_2 = \frac{2a}{\alpha-\beta_2+(\alpha-\beta_1)^{1/2}(\alpha-\beta_2)^{1/2}} \tag{A4}$$

and where $\mathrm{erf}(z)$ is the error function of argument (z). This solution is referred to as the finite-slope solution and is given Andrews & Hanks (1985, appendix C).

The values for the vertical fault offset ($2a$) and fan slopes (β_1, β_2) are calculated from a linear inversion of the profile points away from the degraded scarp (typically points measured beyond 15–30 m either side of the fault scarp). On longer profiles, heights beyond where the fan slope flattens downslope or steepens upslope are discounted in the offset/slope calculations. The reported error in the heights of the individual points on the DGPS profiles is 5–6 cm. An error in the offset is estimated from weighting the points by assuming a constant error of 6 cm for each point. For some estimates of fault vertical offset using short profiles with subsequently few DGPS points away from the scarp to calculate the fan slopes and offset, the 1σ error in the calculated offset can be 30–50%. However, the bulk of offsets >2 m have errors of 3–20%.

The fault offset and fan slopes are then used in Equation (A2) to search for the minimum misfit in the L2-norm sense of the fit of the scarp for κt as a free parameter using the DGPS data points in the centre of the profile (i.e. those points in the near-field that are not used to estimate the fan slopes and fault offset). We assumed an initial scarp angle $\alpha = 35^\circ$ as the angle of repose, with variations of $\pm 5^\circ$ in this assumption having only a small impact on the diffusion age, κt, relative to the spread of the calculated values.

In addition, we checked for the correct identification of the fault position by searching for the minimum misfit in the scarp profile by shifting the choice of fault location by ± 5 m (i.e. the point of the profile at which $x = 0$), re-estimating the fault offset ($2a$) and fan slopes (β_1, β_2) and then recalculating κt for this new location. Of a total of 58 DGPS profiles examined, 12 were excluded from further analysis due to either the profiles being too short to estimate the fan slopes, small offsets that could not be estimated reliably, large erosive channels at the scarp base or profiles which departed strongly from a diffusive shape. For the southern separate rupture, eight of the 12 profiles measured were used to calculate the mean diffusivity.

References

Allard, F. & Erdenebaatar, D. 2005. Khirigsuurs, ritual and mobility in the Bronze Age of Mongolia. *Antiquity*, **79**, 547–563.

Ancuta, L. D., Carlson, R. W., Idleman, B. D. & Zeitler, P. K. 2013. Geochemistry and geochronology of Hangay Dome volcanic rocks: exploring the source of

high topography and volcanism in an intracontinental setting. *Eos, Transactions of the American Geophysical Union Fall Meeting Supplement*, **94**, Abstract T42B-08.

Andrews, D. J. & Hanks, T. C. 1985. Scarp degraded by linear diffusion: inverse solution for age. *Journal of Geophysical Research*, **90**, 10 193–10 208, https://doi.org/10.1029/JB090iB12p10193

Avouac, J.-P. 1993. Analysis of scarp profiles – evaluation of errors in morphologic dating. *Journal of Geophysical Research*, **98**, 6745–6754, https://doi.org/10.1029/92JB01962

Avouac, J.-P. & Peltzer, G. 1993. Active tectonics in southern Xinjiang, China: analysis of terrace riser and normal fault scarp degradation along the Hotan-Qira fault system. *Journal of Geophysical Research*, **98**, 21 773–21 807, https://doi.org/10.1029/93JB02172

Balco, G., Stone, J. O., Lifton, N. A. & Dunai, T. J. 2008. A complete and easily accessible means of calculating erosion rates from ^{10}Be and ^{26}Al measurements. *Quaternary Geology*, **3**, 174–195.

Baljinnyam, I., Bayasgalan, A. *et al.* 1993. *Ruptures of Major Earthquakes and Active Deformation in Mongolia and its Surroundings*. Geological Society of America Memoir, **181**.

Barry, T. L., Saunders, A. D., Kempton, P. D., Windley, B. F., Pringle, M. S., Dorjnamjaa, D. & Saandar, S. 2003. Petrogenesis of Cenozoic Basalts from Mongolia: evidence for the role of asthenospheric v. metasomatized lithospheric mantle sources. *Journal of Petrology*, **44**, 55–91.

Bayasgalan, A., Jackson, J. & McKenzie, D. 2005. Lithosphere rheology and active tectonics in Mongolia: relations between earthquake source parameters, gravity, and GPS measurements. *Geophysical Journal International*, **163**, 1151–1179.

Bucknam, R. C. & Anderson, R. E. 1979. Estimation of fault-scarp ages from a scarp-height slope-angle relationship. *Geology*, **7**, 11–14, https://doi.org/10.1130/0091-7613(1979)7<11:EOFAFA>2.0.CO;2

Calais, E., Vergnolle, M., San'kov, V., Lukhnev, A., Miroshnitchenko, A., Amarjargal, S. & Déverchére, J. 2003. GPS measurements of crustal deformation in the Baikal-Mongolia area (1994–2002): implications for current kinematics of Asia. *Journal of Geophysical Research*, **108**, 2501–2513.

Carretier, S., Ritz, J.-F., Jackson, J. & Bayasgalan, A. 2002. Morphological dating of cumulative reverse fault scarps: examples from the Gurvan Bogd fault system, Mongolia. *Geophysical Journal International*, **148**, 256–277.

Colman, S. M. & Watson, K. 1983. Ages estimated from a diffusion equation model for scarp degradation. *Science*, **221**, 263–265, https://doi.org/10.1126/science.221.4607.263

Crone, A. J., Machette, M. N. & Bowman, J. R. 1997. Episodic nature of earthquake activity in stable continental regions revealed by palaeoseismicity studies of Australian and North American Quaternary faults. *Australian Journal of Earth Sciences*, **44**, 203–214.

Cunningham, W. 2001. Cenozoic normal faulting and regional doming in the southern Hangay region, Central Mongolia: implications for the origin of the Baikal rift province. *Tectonophysics*, **331**, 389–411.

Deng, Q. & Liao, Y. 1996. Paleoseismology along the range-front fault of Helan Mountains, north central China. *Journal of Geophysical Research*, **101**, 5873–5893.

Desilets, D. & Zreda, M. 2003. Spatial and temporal distribution of secondary cosmic-ray nucleon intensities and applications to in situ cosmogenic dating. *Earth and Planetary Science Letters*, **206**, 21–42.

Desilets, D., Marek, Z. & Prabu, T. 2006. Extended scaling factors for in situ cosmogenic nuclides: new measurements at low latitude. *Earth and Planetary Science Letters*, **246**, 265–276.

Dunai, T. J. 2001. Influence of secular variation of the geomagnetic field on production rates of in situ produced cosmogenic nuclides. *Earth and Planetary Science Letters*, **193**, 197–212.

Elliott, J. R., Walters, R. J., England, P. C., Jackson, J. A., Li, Z. & Parsons, B. 2010. Extension on the Tibetan plateau: recent normal faulting measured by InSAR and body wave seismology. *Geophysical Journal International*, **83**, 503–535, https://doi.org/10.1111/j.1365-246X.2010.04754.x

Farr, T. G. & Kobrick, M. 2000. Shuttle radar topography mission produces a wealth of data. *EOS,* **81**, 583–585.

Filippov, L. V., Lipovskiy, Y. O. & Kapitonova, T. A. 1976. Central Mongolian potassic basaltoids and abyssal magma formation. *Geochemistry International*, **13**, 106–118.

Florensov, N. A. & Solonenko, V. P. (eds) 1965. *The Gobi-Altay earthquake*. Moscow Akademiya Nauk USSR, **391** [in Russian, English translation by Israel Program for Scientific Translations].

Frankel, K. L., Wegmann, K. W. *et al.* 2010. Late Pleistocene slip rate of the Höh Serh–Tsagaan Salaa fault system, Mongolian Altai and intracontinental deformation in central Asia. *Geophysical Journal International*, **183**, 1134–1150, https://doi.org/1110.1111/j.1365-1246X.2010.04826.x

Hanks, T. C. 2000. The age of scarplike landforms from diffusion-equation analysis. *In*: Noller, J. S., Sowers, J. M. & Lettis, W. R. (eds) *Quaternary Geochronology: Methods and Applications*, **4**, American Geophysical Union, Washington, DC, https://doi.org/10.1029/RF004p0313

Hanks, T. C. & Andrews, D. J. 1989. Effect of far-field slope on morphologic dating of scarplike landforms. *Journal of Geophysical Research*, **94**, 565–573, https://doi.org/10.1029/JB094iB01p00565

Hilley, G. E., DeLong, S., Prentice, C., Blisniuk, K. & Arrowsmith, R. 2010. Morphologic dating of fault scarps using airborne laser swath mapping (ALSM) data. *Geophysical Research Letters*, **37**, L04301, https://doi.org/10.1029/2009GL042044

Heisinger, B., Lal, D., Jull, A. J. T., Kubik, P., Ivy-Ochs, S., Knie, K. & Nolte, E. 2002*a*. Production of selected cosmogenic radionuclides by muons: 2. Capture of negative muons. *Earth and Planetary Science Letters*, **200**, 357–369.

Heisinger, B., Lal, D. *et al.* 2002*b*. Production of selected cosmogenic radionuclides by muons 1. Fast

muons. *Earth and Planetary Science Letters*, **200**, 345–355.

Hunt, A. C., Parkinson, I. J., Harris, N. B. W., Barry, T. L., Rogers, N. W. & Yondon, M. 2012. Cenozoic volcanism on the Hangai Dome, Central Mongolia: geochemical evidence for changing melt sources and implications for mechanisms of melting. *Journal of Petrology*, **53**, 1913–1942.

Ionov, D. A. 2007. Compositional variations and heterogeneity in fertile lithospheric mantle: peridotite xenoliths in basalts from Tariat, Mongolia. *Contributions to Mineralogy and Petrology*, **154**, 455–477.

Jackson, J. A. & Blenkinsop, T. 1997. The Bilila-Mtakataka fault in Malawi: an active 100 km long, normal fault segment in thick seismogenic crust. *Tectonics*, **16**, 137–150.

Jackson, J. A. & White, N. J. 1989. Normal faulting in the upper continental crust: observations from regions of active extension. *Journal of Structural Geology*, **11**, 15–36.

Khil'ko, S. D., Kurushin, R. A. *et al.* 1985. Strong earthquakes, paleoseismogeological and macroseismic data. *Earthquakes and the Base for Seismic Zoning of Mongolia*. The Joint Soviet–Mongolian 41Scientific Geological Research Expedition Transactions, **41**.

Koehler, R. D. & Wesnousky, S. G. 2011. Late Pleistocene regional extension rate derived from earthquake geology of late Quaternary faults across the Great Basin, Nevada, between 38.5N and 40 N latitude. *Geological Society of America Bulletin*, **123**, 631–650, https://doi.org/10.1130/B30111.1

Kurushin, R. A., Bayasgalan, A. *et al.* 1997. *The Surface Rupture of the 1957 Gobi–Altay, Mongolia, Earthquake*. Geological Society of America, Special Papers, **320**.

Lal, D. 1991. Cosmic ray labeling of erosion surfaces: in situ nuclide production rates and erosion models. *Earth and Planetary Science Letters*, **104**, 424–439.

Lifton, N. A., Bieber, J. W., Clem, J. M., Duldig, M. L., Evenson, P., Humble, J. E. & Pyle, R. 2005. Addressing solar modulation and long-term uncertainties in scaling secondary cosmic rays for in situ cosmogenic nuclide applications. *Earth and Planetary Science Letters*, **239**, 140–161.

Mattson, A. & Bruhn, R. L. 2001. Nonlinear diffusion-equation modelling of Quaternary fault morphology: Wasatch fault zone and eastern Great Basin. *Journal of Geophysical Research*, **106**, 13 739–13 750.

Natsag-Yum, L., Balzhinnyam, I. & Monhoo, D. 1971. Mongolian earthquakes. *In*: *Seismic Regionalization of Ulan Bator*. Nauka, Moscow, 54–82 [in Russian].

Nishiizumi, K., Imamura, M., Caffee, M., Southon, J., Finkel, R. & McAnich, J. 2007. Absolute calibration of ^{10}Be AMS standards. *Nuclear Instruments and Methods in Physics Research B*, **258**, 403–413.

Nissen, E., Emmerson, B. *et al.* 2007. Combining InSAR and seismology to study the 2003 Siberian Altai earthquakes – dextral strike-slip and anticlockwise rotations in the northern India-Eurasia collision zone. *Geophysical Journal International*, **169**, 216–232.

Petit, C., Koulakov, I. & Déverchère, J. 1998. Velocity structure around the Baikal rift zone from teleseismic and local earthquake traveltimes and geodynamic implications. *Tectonophysics*, **296**, 125–144.

Phillips, F. M., Ayarbe, J. P., Harrison, J. B. J. & Elmore, D. 2003. Dating rupture events on alluvial fault scarps using cosmogenic nuclides and scarp morphology. *Earth and Planetary Science Letters*, **215**, 203–218, https://doi.org/10.1016/S0012-821X(03)004199

Ramsey, C. B. & Lee, S. 2013. Recent and planned developments of the program OXCAL. *Radiocarbon*, **55**, 720–730.

Reimer, P. J., Bard, E. *et al.* 2013. IntCal13 and Marine13 radiocarbon age calibration curves 0–50,000 years cal BP. *Radiocarbon*, **55**, 1869–1887.

Rizza, M., Ritz, J. F. *et al.* 2011. Slip rate and slip magnitudes of past earthquakes along the Bogd left-lateral strike-slip fault (Mongolia). *Geophysical Journal International*, **186**, 897–927.

Rizza, M., Ritz, J. F. *et al.* & Aster Team 2015. Earthquake geology of the Bulnay Fault (Mongolia). *Bulletin of the Seismological Society of America*, **105**, 10.1785/0120140119

Schlische, R. W., Young, S. S., Ackermann, R. V. & Gupta, A. 1996. Geometry and scaling relations of a population of very small rift-related normal faults. *Geology*, **24**, 683–686.

Schlupp, A. 1996. *Neotectonique de la Mongolie occidentale analyse a partier de donnees de terrain, sismologiques et satellitaires*. PhD thesis, Universite Louis Pasteur, Ecole et Observatoire de Physique de Globe de Strasbourg [in French].

Schlupp, A. & Cisternas, A. 2007. Source history of the great Mongolian earthquakes (Tsetserleg, Bolnay). *Geophysical Journal International*, **169**, 1115–1131.

Scholz, C. H., Aviles, C. & Wesnousky, S. 1986. Scaling differences between large intraplate and interplate earthquakes. *Bulletin of the Seismological Society of America*, **76**, 65–70.

Spelz, R. M., Fletcher, J. M., Owen, L. A. & Caffee, M. W. 2008. Quaternary alluvial-fan development, climate and morphologic dating of fault scarps in Laguna Salada, Baja California, Mexico. *Geomorphology*, **102**, 578–594, https://doi.org/10.1016/j.geomorph.2008.06.001

Stone, J. O. 2000. Air pressure and cosmogenic isotope production. *Journal of Geophysical Research*, **105**, 23 753–23 759.

Stover, C. W. & Coffman, J. L. 1993. *Seismicity of the United States, 1568–1989 (revised)*. US Government Printing Office, Washington DC, USA.

Stuiver, M. & Polach, H. A. 1977. Discussion; reporting of C-14 data. *Radiocarbon*, **19**, 355–363.

Tielke, J. A., Kastl, B. C. & Otgonhuu, J. 2007. Genesis and evolution of Tertiary lavas of the central Hangay Mountains, Mongolia. *In*: Bettison-Varga, L. (ed.) *20th Annual Keck Research Symposium in Geology Proceedings*. Keck Geology Consortium, Wooster, OH, 14–24.

Vassallo, R. 2006. *Chronologie et evolution des reliefs dans la region de Mongolie-Siberie: approche morphotectonique et geochronologique*. PhD thesis, Universite Montpellier II, Montpellier [in French].

Vassallo, R., Jolivet, M. *et al.* 2007. Uplift age and rates of the Gurvan Bogd system (Gobi-Altay) by

apatite fission track analysis. *Earth and Planetary Science Letters*, **259**, 333–346.

WALKER, R. T., BAYASGALAN, A. *ET AL*. 2006. Geomorphology and structure of the Jid right-lateral strike-slip fault in the Mongolian Altay Mountains. *Journal of Structural Geology*, **28**, 1607–1622.

WALKER, R. T., NISSEN, E., MOLOR, E. & BAYASGALAN, A. 2007. A re-interpretation of the active faulting in central Mongolia. *Geology*, **35**, 759–762.

WALKER, R. T., MOLOR, E., FOX, M. & BAYASGALAN, A. 2008. Active tectonics of an apparently aseismic region: distributed active strike-slip faulting in the Hangay Mountains of central Mongolia. *Geophysical Journal International*, **174**, 1121–1137, https://doi.org/10.1111/j.1365-246X.2008.03874.x

WALLACE, R. E. 1977. Profiles and ages of young fault scarps, north-central Nevada. *Geological Society of America Bulletin*, **88**, 1267–1281.

WALLACE, R. E. 1989. Fault plane segmentation in brittle crust and anisotropy in loading system. *In*: SCHWARTZ, D. P. & SIBSON, R. H. (eds) *Fault Segmentation and Controls on Rupture Initiation and Termination*. US Geological Survey Open-File Report **89-315**, 400–408.

WELLS, D. L. & COPPERSMITH, K. J. 1994. New empirical relationships among magnitude, rupture length, rupture width, rupture area, and surface displacement. *Bulletin of the Seismological Society of America*, **84**, 974–1002.

WINDLEY, B. & ALLEN, M. 1993. Mongolian plateau: evidence for a late Cenozoic mantle plume under central Asia. *Geology*, **21**, 295–298.

WEST, A. J., FOX, M., WALKER, R. T., CARTER, A., HARRIS, T., WATTS, A. B. & GANTULGA, B. 2013. Links between climate, erosion, uplift, and topography during intracontinental mountain building of the Hangay Dome, Mongolia. *Geochemistry, Geophysics, Geosystems*, **14**, https://doi.org/10.1002/2013GC004859

WESTOBY, M. J., BRASINGTON, J., GLASSER, N. F., HAMBREY, M. J. & REYNOLDS, J. M. 2012. 'Structure-from-Motion' photogrammetry: a low-cost, effective tool for geoscience applications. *Geomorphology*, **179**, 300–314.

WRIGHT, J. 2007. Organizational principles of Khirigsuur monuments in the lower Egiin Gol valley, Mongolia. *Journal of Anthropological Archaeology*, **26**, 350–365.

YANSHIN, A. L. 1975. *Mesozoic and Cenozoic Tectonics and the Magmatism of Mongolia*. Joint Soviet–Mongolian Scientific Research Geological Expedition Transactions, **11** [in Russian].

YARMOLYUK, V. V., KUDRYASHOVA, E. A., KOZLOVSKY, A. M. & LEBEDEV, V. A. 2008. Late Cenozoic volcanism of Khangai (Central Mongolia): evidence for recent orogeny in Central Asia. *Doklady Earth Sciences*, **422**, 1032–1036.

YUAN, T. H., FENG, X. J. & DENG, B. Z. 1991. *The 1556 Huaxian Earthquake*. Earthquake Press, China [in Chinese].

ZHANG, B., LIAO, Y., GUO, S., WALLACE, R. E., BUCKNAM, R. C. & HANKS, T. C. 1986. Fault scarps related to the 1739 earthquake and seismicity of the Yinchuan graben, Ningxia Huizu Zizhiqu, China. *Bulletin of the Seismological Society of America*, **76**, 1253–1287.